

Baseline vector repeatability at the sub-millimeter level enabled by radio interferometer phase delays of intra-site baselines

Ming H. Xu^{1,2,10}, Tuomas Savolainen^{1,2}, Sergei Bolotin³, Simone Bernhart⁴,
Christian Plötz⁵, Rüdiger Haas⁶, Eskil Varenius⁶, Guangli Wang⁷, Jamie
McCallum⁸, Robert Heinkelmann⁹, Susanne Lunz¹⁰, Harald Schuh^{10,9},
Nataliya Zubko¹¹, and Niko Kareinen¹¹

¹Aalto University Metsähovi Radio Observatory, Metsähovintie 114, 02540 Kylmälä, Finland

²Aalto University Department of Electronics and Nanoengineering, PL15500, FI-00076 Aalto, Finland

³NVI Inc. at NASA Goddard Space Flight Center, Code 61A.0, Greenbelt, MD, 20771, USA

⁴Reichert GmbH/Bundesamt für Kartographie und Geodäsie, 53121 Bonn, Germany

⁵Geodetic Observatory Wettzell, Federal Agency for Cartography and Geodesy, Sackenrieder Str. 25,
93444 Bad Kötzing, Germany

⁶Department of Space, Earth and Environment, Onsala Space Observatory, Chalmers University of
Technology, 439 92 Onsala, Sweden

⁷Shanghai Astronomical Observatory, Chinese Academy of Sciences, No. 80 Nandan Road, 200030,
Shanghai, P. R. China

⁸School of Natural Sciences, University of Tasmania, Private Bag 37, Hobart TAS 7001, Australia

⁹Deutsches GeoForschungsZentrum (GFZ), Potsdam, Telegrafenberg, A17, 14473 Potsdam, Germany

¹⁰Institute of Geodesy and Geoinformation Science, Technische Universität Berlin, Straße des 17. Juni
135, 10623, Berlin, Germany

¹¹Finnish Geospatial Research Institute, Geodeetinrinne 2, FIN-02430 Masala, Finland

Key Points:

- Baseline vectors of legacy antennas and co-located, new antennas are obtained from phase delays with the highest possible accuracy.
- Sources of error in short-baseline observations are investigated at the 1 mm level.

Abstract

We report the results of position ties for short baselines at eight geodetic sites based on phase delays that are extracted from global geodetic very-long-baseline interferometry (VLBI) observations rather than dedicated short-baseline experiments. An analysis of phase delay observables from two antennas at the Geodetic Observatory Wettzell, Germany, extracted from 107 global 24-hour VLBI sessions since 2019 yields weighted root-mean-square scatters about the mean baseline vector of 0.3, 0.3, and 0.8 mm in the east, north, and up directions, respectively. Position ties are also obtained for other short baselines between legacy antennas and nearby, newly built antennas. They are critical for maintaining a consistent continuation of the realization of the terrestrial reference frame, especially when including the new VGOS network. The phase delays of the baseline WETTZ13N–WETTZELL enable an investigation of sources of error at the sub-millimeter level. We found that a systematic variation of larger than 1 mm can be introduced to the up estimates of this baseline vector when atmospheric delays were estimated. Although the sub-millimeter repeatability has been achieved for the baseline vector WETTZ13N–WETTZELL, we conclude that long term monitoring should be conducted for more short baselines to assess the instrumental effects, in particular the systematic differences between phase delays and group delays, and to find common solutions for reducing them. This will be an important step towards the goal of global geodesy at the 1 mm level.

Plain Language Summary

We report the results of position ties for short baselines at eight geodetic sites based on phase delays that are extracted from global geodetic very-long-baseline interferometry (VLBI) observations rather than dedicated short-baseline experiments. By using the inherently more precise observables - phase delays, a baseline vector repeatability of WETTZ13N–WETTZELL has been achieved at the sub-millimeter level for the horizontal directions and at the 1 millimeter (mm) level for the vertical direction based on VLBI experiments of 107 days during 3.5 years. Position ties based on phase delays are also obtained for other short baselines between legacy antennas and nearby, newly built antennas, and they are critical to maintain a consistent continuation of the realization of terrestrial reference frame into the future of a network of these new antennas. We have evaluated the instrumental stability at the 1 mm level, which is an important step towards the goal of global geodesy at this level.

1 Introduction

The technique of very-long-baseline interferometry (VLBI) combines the signal of a radio source recorded by a pair of radio antennas to provide the delay, both phase delay and group delay, of the arrival times at the two antennas. It was initially developed for astronomy in the late 1960s to derive high angular resolution images for celestial objects and was later also used for geodesy to determine the orientation of the Earth in space and the positions of the antennas on the Earth with a high precision (see, [Sovers et al., 1998](#), and the references therein). In astronomy, the highest accuracy is obtained by making use of the full precision of phase delays for relative measurements between pairs of nearby objects on the sky. Phase delays can be also used in geodesy to obtain relative positions between nearby antennas on the Earth with the highest accuracy.

In the transition period of the geodetic VLBI systems, phase delays of short baselines enable significant scientific applications. Many antennas of the legacy VLBI system which is mainly based on dual-band observations (2.3 GHz and 8.4 GHz), though being continuously upgraded and still used, have reached the limits of their capability; this legacy system is pushed to the limits also because the Earth science studies

78 continue to pursue more precise geodetic measurements. The next-generation geode-
 79 tic VLBI system, known as the VLBI Global Observing System (VGOS; Niell et al.,
 80 2007; Petrachenko et al., 2009), has been developing worldwide with antennas of rela-
 81 tively small diameter, 12–13 m, and broadband receivers, 2.0–14.0 GHz, with the
 82 aim to achieve 1 mm station position accuracy and 0.1 mm/yr velocity stability on
 83 global scales. It is necessary to accurately tie these new, small antennas to the legacy,
 84 co-located antennas that have a long observing history since 1979 and have been play-
 85 ing a fundamental role in the realizations of the International Terrestrial Reference
 86 Frame (ITRF; Altamimi et al., 2016) to allow for a consistent continuation of the
 87 ITRF into the VGOS era. Recently, dedicated position tie measurements of this
 88 type have been performed, for instance, for the legacy antenna and the VGOS an-
 89 tenna at the Kokee Park Geophysical Observatory by Niell et al. (2021) and for the
 90 legacy antenna and the twin VGOS antennas at the Onsala Space Observatory by
 91 Varenius et al. (2021). An alternative way to derive these position ties is to make
 92 use of the global geodetic VLBI observations by the International VLBI Service for
 93 Geodesy and Astrometry (IVS; Schuh & Behrend, 2012; Nothnagel et al., 2017, see
 94 <https://ivscc.gsfc.nasa.gov/index.html>).

95 In this work, we analyze the observed phase delays to obtain position ties for as
 96 many co-located legacy and VGOS-compatible antennas and as many observations as
 97 possible. Our purpose is twofold: (1) to determine the baseline vectors between the
 98 legacy antennas and the co-located, new antennas with the highest possible accuracy
 99 and (2) to investigate the baseline vector repeatability of the short baselines determined
 100 from a time series of VLBI observations. The latter will allow us to separate the purely
 101 instrumental effects, affecting both short-baseline and long-baseline observables and
 102 dominating the estimates of the short-baseline vectors, from other contributions due to
 103 geophysical/astrophysical effects. The goal of this study is to contribute to the effort
 104 of the consistent continuation of the global Terrestrial Reference Frame (TRF) and to
 105 investigate the sources of error, mainly the instrumental effects, in VLBI observations.

106 2 Data and data analysis

107 We analyzed the IVS observations to derive the position ties for the antennas
 108 shown in Fig. 1. The routine geodetic solutions of these global sessions have already
 109 been submitted by IVS analysis centers to the IVS combination center, which com-
 110 bines the results and provides the VLBI inputs for building the ITRF. (For the
 111 latest ITRF2020, the IVS analysis activities can be found at [https://ivscc.gsfc](https://ivscc.gsfc.nasa.gov/IVS_AC/IVS-AC_ITRF2020.htm)
 112 [.nasa.gov/IVS_AC/IVS-AC_ITRF2020.htm](https://ivscc.gsfc.nasa.gov/IVS_AC/IVS-AC_ITRF2020.htm).) However, the short-baseline observables
 113 in these global geodetic VLBI observations can be analyzed independently from the
 114 observations of the entire network in each session in order to obtain the baseline vectors
 115 with the highest accuracy. The reasons are as follows:

- 116 1. In the routine geodetic VLBI solutions, observables at both S and X band are re-
 117 quired to remove the dispersion affecting the radio signal when it passes through
 118 the charged medium, mainly the ionosphere. Any local radio interference, which
 119 is highly correlated for antennas at the same site, contributes large noise to the
 120 S band observables and thus to the ionospheric-free observables, though scaled
 121 down by a factor of 13.8. More importantly, false detections at S band lead to
 122 flagging the corresponding observables at X band as bad, and in not uncommon
 123 cases the observations of an antenna in one session are completely lost in the
 124 final data analysis due to the issues that happened only at S band. (See the
 125 comparison for baseline NYALES13S–NYALES20 in Sect. 3.1.2.) However, the ob-
 126 servables at S band are not needed for short baselines, as the ionospheric effect
 127 is negligible for co-located antennas (pointing to a common source).

- 128 2. The position estimates of the co-located antennas treated independently in a
 129 geodetic solution of a full session are affected by systematic error sources, such
 130 as source structure, ionosphere, and atmosphere. In contrast, these systematic
 131 errors impose minimum impacts on the short-baseline observables.
- 132 3. Thermal noise can be one of the dominant errors in the short-baseline group
 133 delay observables, and it is significantly reduced by using phase delay observables
 134 (Ray & Corey, 1991).
- 135 4. Some of these short baselines are regularly scheduled in the VLBI sessions having
 136 a duration of one hour for the rapid determination of the highly variable Earth's
 137 rotation, called Intensive sessions, which by their design are not intended to be
 138 used for deriving station positions. They allow us to investigate the position
 139 accuracy that can be obtained from short-time observations, like the Intensive
 140 sessions.

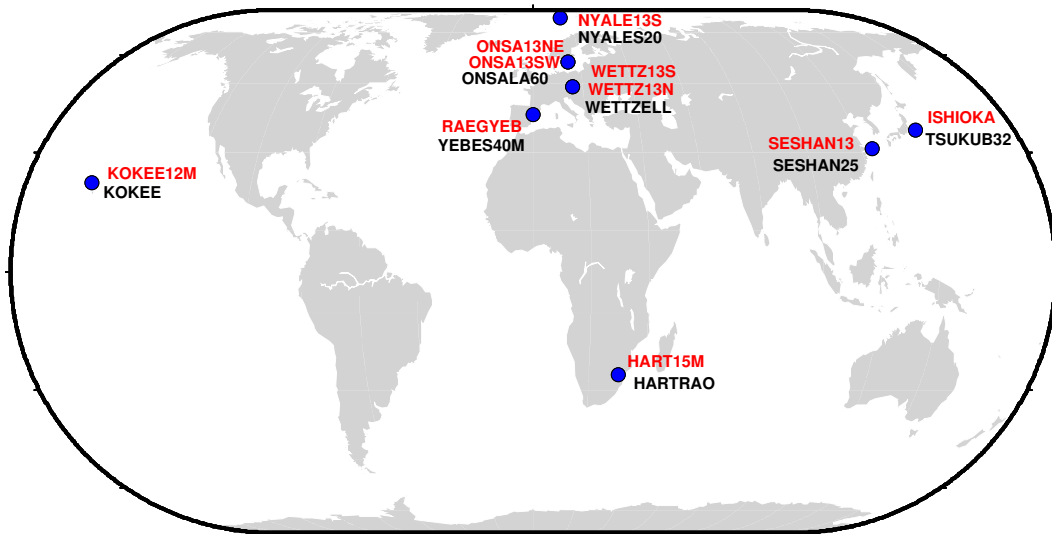


Figure 1. Radio telescopes with position tie measurements reported in this study. At each VLBI site (blue dot), there is a legacy telescope (black designator) and at least one new telescope (red designator).

141 2.1 Observations

142 In addition to the dedicated experiments for the Onsala antennas (the ONTIE
 143 sessions) that were reported in Varenius et al. (2021) and the Kokee antennas re-
 144 ported in Niell et al. (2021), short-baseline observations were found in three types
 145 of geodetic sessions: regular 24-hour sessions, special sessions of a combined net-
 146 work from legacy antennas and VGOS antennas, and Intensive sessions. The total
 147 number of the VLBI sessions (of these three types) analyzed in this study and the
 148 baseline lengths are reported in Table 1. Baseline ONSA13NE–ONSA13SW is formed by
 149 two VGOS antennas; each of the other ten baselines consists of a legacy antenna
 150 and a new antenna with a small diameter in the 12–15 m range. The broadband
 151 receivers used in the VGOS system record the linearly polarized components of a
 152 signal, denoted by H and V , whereas the receivers of the legacy antennas are de-
 153 signed to record right-hand circular polarization, denoted by R . In the current data
 154 processing of VGOS observations, the pseudo-Stokes I visibilities are formed from
 155 the four linear polarization correlation products due to lack of knowledge of the cross-

156 polarization “D” terms (see [https://www.haystack.mit.edu/wp-content/uploads/](https://www.haystack.mit.edu/wp-content/uploads/2020/07/docs_hops.000_vgos-data-processing.pdf)
 157 [2020/07/docs_hops.000_vgos-data-processing.pdf](https://www.haystack.mit.edu/wp-content/uploads/2020/07/docs_hops.000_vgos-data-processing.pdf)). For a mixed baseline of a
 158 legacy antenna and a VGOS antenna, a combined product of $RH+RV$ is formed;
 159 the observations including these baselines in the network are referred to as the mixed-
 160 mode sessions. For the observations analyzed in this work, the first five baselines of
 161 Table 1 were observed in legacy S/X mode, and the remaining six baselines were ob-
 162 served in mixed mode. The new antennas involved in the first five baselines may have
 163 observed with a broadband receiver in other sessions or may be upgraded as a VGOS
 164 antenna in the future.

Table 1. Short baselines analyzed in the study, the numbers of sessions, and the baseline lengths.

Baseline	2-letter code ¹	Number of sessions	Length (m)
WETTZ13N–WETTZELL	Wn–Wz	165 ²	123
NYALE13S–NYALES20	Ns–Ny	19	1539
ISHIOKA–TSUKUB32	Is–Ts	17	16606
HARTRAO–HART15M	Hh–Ht	8	113
SESHAN13–SESHAN25	S6–Sh	1	56
WETTZ13S–WETTZELL	Ws–Wz	2	187
RAEGYEB–YEBES40M	Yj–Ys	1	194
KOKEE12M–KOKEE	K2–Kk	1	31
ONSALA60–ONSA13SW	On–Ow	2	540
ONSA13NE–ONSALA60	Oe–On	1	469
ONSA13NE–ONSA13SW	Oe–Ow	1	75

¹The 2-letter codes of geodetic VLBI antennas are available from <https://cddis.nasa.gov/archive/vlbi/ivscontrol/ns-codes.txt>. ²These consist of 107 global 24-hour sessions and 58 Intensives. The complete VLBI session list per year is available from <https://ivscc.gsfc.nasa.gov/program/master.html>.

165 2.2 Phase ambiguity

166 For geodetic VLBI observations in the legacy mode and the mixed mode, a multi-
 167 dimensional Fourier search from fringe phases of an interferometer gives (multi-band)
 168 group delay, delay rate, and visibility phase. The group delay is the derivative of
 169 phase with respect to frequency, whereas the phase delay is obtained as the ratio of
 170 the visibility phase to frequency. Phase delays intrinsically have higher precision than
 171 group delays, however, they are typically not used in routine geodetic solutions due to
 172 unknown phase turns, i.e. phase ambiguities.

173 Phase delay differs from group delay in terms of (1) the instrumental effects, such
 174 as the rotation of the feeds, the dispersion of the signal in the antenna system itself,
 175 and the signal delays in the waveguides prior to the injection of the phase calibration
 176 signals, (2) the frequency-dependent astronomical effects, the dispersive nature of the
 177 plasma along the line of sight and extended structure of radio sources, and (3) the
 178 magnitude of the thermal noise. The instrumental effects, which can be very large,
 179 either can be calibrated or are expected to be constant. The integrated plasma densities
 180 along the line of sight have very small differences for the co-located antennas of a short
 181 baseline. Most of the radio sources in the geodetic catalog, after a refinement over 40
 182 years, are compact at the arcsecond scale, and the effects of structure for the majority
 183 of the sources at the scale of milli-arcsecond are relatively small for the short-baseline

184 observations (see, e.g., [Xu et al., 2016, 2019](#)). For short baselines, the uncertainties of
 185 group delays due to thermal noise are generally far smaller than the phase ambiguity
 186 spacing. In the cases where the group delays are very noisy, for instance on the baseline
 187 NYALE13S–NYALES20, theoretical delays instead of the group delay observables can be
 188 used for directly aligning the phases over time, assuming that the unpredictable effects
 189 on the short baselines change relatively smoothly. Exceptional cases can happen when
 190 antennas have very unstable clocks or the a priori station position is very poorly
 191 known. The third option is to do a geodetic solution based on group delay observables
 192 for estimating the clock parameters and the station positions and then to employ them
 193 to connect the phases for resolving phase ambiguities.

194 The delay spacing of the phase ambiguities is about 120 ps at X band and about
 195 450 ps at S band. In general, the variation of the differences between phase delays and
 196 group delays are expected to be relatively small compared to the ambiguity spacing, so
 197 that it is straightforward for most of the sessions to connect the phases over time. Yet
 198 there can still be (ambiguous) constant offsets between phase delays and group delays,
 199 which will be fully absorbed by the estimated clock offsets. (We should note that
 200 resolving phase ambiguity is generally challenging for long baselines because of the
 201 impacts of, for instance, atmosphere.) In this study about short baselines, we used the
 202 group delays to eliminate the 2π phase ambiguity of the corresponding phase delays
 203 and afterward examined the differences between the group delays and the phase delays
 204 for all observations of a baseline in a session. If the differences over time follow the
 205 pattern of a smooth curve with a scatter significantly smaller than half the ambiguity
 206 spacing, it is an indication of successful elimination of phase ambiguities, while a
 207 failure would be obvious through a random distribution of the differences within the
 208 ambiguity spacing. This method was used as an initial inspection. The other methods
 209 were used as alternatives for some of the baselines.

210 When phase calibration signals are too weak to be useful (or not available) for
 211 removing the instrumental phase variations between various frequency channels, the
 212 observations of radio sources with high flux densities can be used as an alternative
 213 to calibrate the instrumental phases, which makes the fringe fitting of group delays
 214 possible. This process is referred to as manual phase calibration. However, in this case
 215 one may not be able to connect the phases because of the variations of instrumental
 216 phases over time. The details of the correlation process are written in the IVS corre-
 217 lator reports. The feed rotation angle (FRA) corrections need to be considered even
 218 for these very short baselines, since the two antennas at one site can have different
 219 mounting types leading to differences in the FRA corrections, as is the case for the
 220 two antennas HARTRAO and HART15M (equatorial/altazimuth).

221 **2.3 Comparison of group delays and phase delays**

222 The differences between phase delays and group delays can be investigated after
 223 resolving phase ambiguities. These differences are shown in Fig. 2 for four cases as
 224 examples, which demonstrate that phase ambiguities can be reliably resolved based on
 225 group delay observables.

226 There can be systematic variations in the differences, which can change as much
 227 as 100 ps over an hour, as shown for baseline WETTZ13N–WETTZELL in session 21MAY10XA.
 228 When estimating only a constant clock offset and a clock rate over the 24 hours (two
 229 parameters), the delay residuals from a solution of group delays in the session have a
 230 similar pattern as the differences between group delays and phase delays, whereas the
 231 delay residuals based on phase delays are much smaller and flat. The delay residu-
 232 als are shown in Fig. S1 of the supporting information. This result strongly suggests
 233 that the differences are introduced by the group delays. They are largely absorbed
 234 by the clock parameters in a full geodetic solution. These effects may be caused by

235 the dispersion effects in the waveguides of the receivers prior to the injection of phase
 236 calibration signals, the undesired wave reflections within the antennas, and spurious
 237 phase calibration signals (see, e.g., [Rogers, 1991](#)). Note that instrumental instabilities
 238 of this size will cause difficulties for resolving phase ambiguities of the observations
 239 on long baselines including one of these two antennas. This is one of the obstacles
 240 when resolving phase ambiguities for global geodetic VLBI observations and will be
 241 discussed in a future study. Such large variability occurs in other sessions including
 242 this baseline and in observations of other short baselines as well. The systematic vari-
 243 ations, though much smaller, are also visible on baseline HARTRAO–HART15M in South
 244 Africa and baseline ISHIOKA–TSUKUB32 in Japan. Recovering phase ambiguities for an
 245 intensive session is shown in the bottom panel of Fig. 2.

246 Based on closure analysis (see, e.g., [Xu et al., 2016](#); [Anderson & Xu, 2018](#); [Xu et
 247 al., 2021](#)), the inherently higher precision of phase delays can be seen directly at the
 248 observable level without a geodetic solution. Figure 3 shows the closure phase delays
 249 and closure group delays of triangle ONSA13NE–ONSA13SW–ONSALA60 in session ON0080
 250 (March 20, 2020). In principle, closures are sensitive only to the thermal noise and
 251 the effects of source structure, although the latter imposes minimum impacts on the
 252 observations of this small triangle for most of the geodetic sources. The unweighted
 253 and the weighted root-mean-square (rms) are 21.1 ps and 13.2 ps for the closure group
 254 delays, respectively, and they are 7.5 ps and 6.8 ps for the closure phase delays. Given
 255 that the thermal noise is independent among the three baselines, the noise level is
 256 about 12 ps in the group delays and 4 ps in the phase delays. Considering that the
 257 dominating source of error in the short-baseline observables is the thermal noise, this
 258 improvement in the accuracy of observables can lead to significantly better results.

259 2.4 Ionospheric corrections

260 The assumption that the ionospheric effect on short baseline is negligible can be
 261 validated after resolving phase ambiguities for both S band and X band observables.
 262 For baseline WETTZ13N–WETTZELL in session 21MAY10XA (a session with typical iono-
 263 spheric delay corrections), the rms scatter of the ionospheric corrections at X band
 264 about the mean value, derived from the combination of the phase delays at S and X
 265 band, is less than 1 ps, and the peak-to-peak fluctuation is 3 ps. For baseline NYALE13S–
 266 NYALES20, about 1.5 km apart, the rms scatter is 2 ps with the peak fluctuation of 10 ps
 267 in session 21JUN24XE. For baseline ISHIOKA–TSUKUB32, about 16.6 km apart, the rms
 268 scatter and the fluctuation in session 16DEC20XA are similar to the values for the
 269 baseline NYALE13S–NYALES20.

270 In order to assess how much the S band observables corrupt the short-baseline
 271 observables in routine geodetic solutions, the rms scatters of the ionospheric corrections
 272 at X band, derived from the group delays at S and X band in the conventional way
 273 and restored in the databases, are calculated for the short baselines in the mixed
 274 mode session RD2005. The rms scatter is 15 ps with the peak fluctuation of about
 275 100 ps for baseline WETTZ13S–WETTZELL of 0.2 km length and is 90 ps with the peak
 276 fluctuation of about 600 ps for baseline ONSALA60–ONSA13SW of 0.5 km length. As a
 277 direct comparison, the rms scatter of the ionospheric corrections in the IVS database
 278 of session 21JUN24XE for baseline NYALE13S–NYALES20 is 120 ps. However, this is
 279 about two orders of magnitude larger than the real contribution of the ionospheric
 280 effects, as determined above by using the phase delays at the two bands. With this
 281 justification, the phase delays at S band were not used in our solutions because they
 282 can lead to flagging as outliers a significant amount of usable X band phase delays.

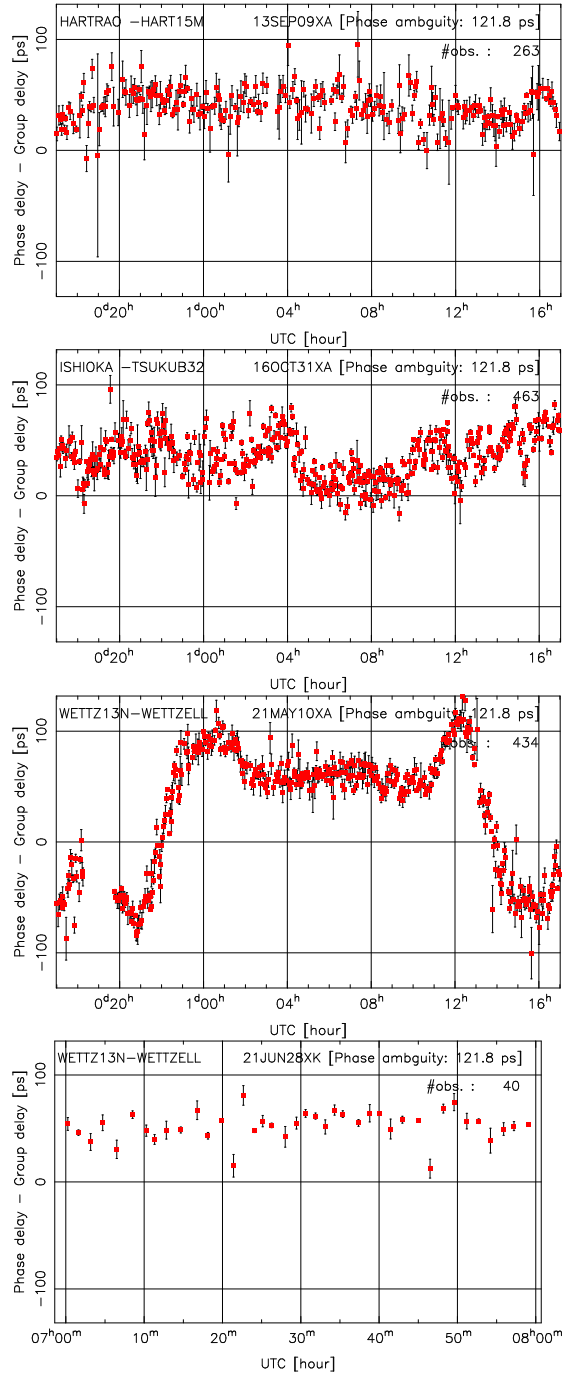


Figure 2. Demonstration of the differences between group delays and phase delays for baselines HARTRAO-HART15M (top), ISHIOKA-TSUKUB32 (middle top), and WETTZ13N-WETTZELL (middle bottom) in 24-hour sessions and for baseline WETTZ13N-WETTZELL in a 1-hour session (bottom). Error bars shown are the combined uncertainties of the phase delays and the group delays. The plotting scale corresponds to about minus and plus one turn of phase.

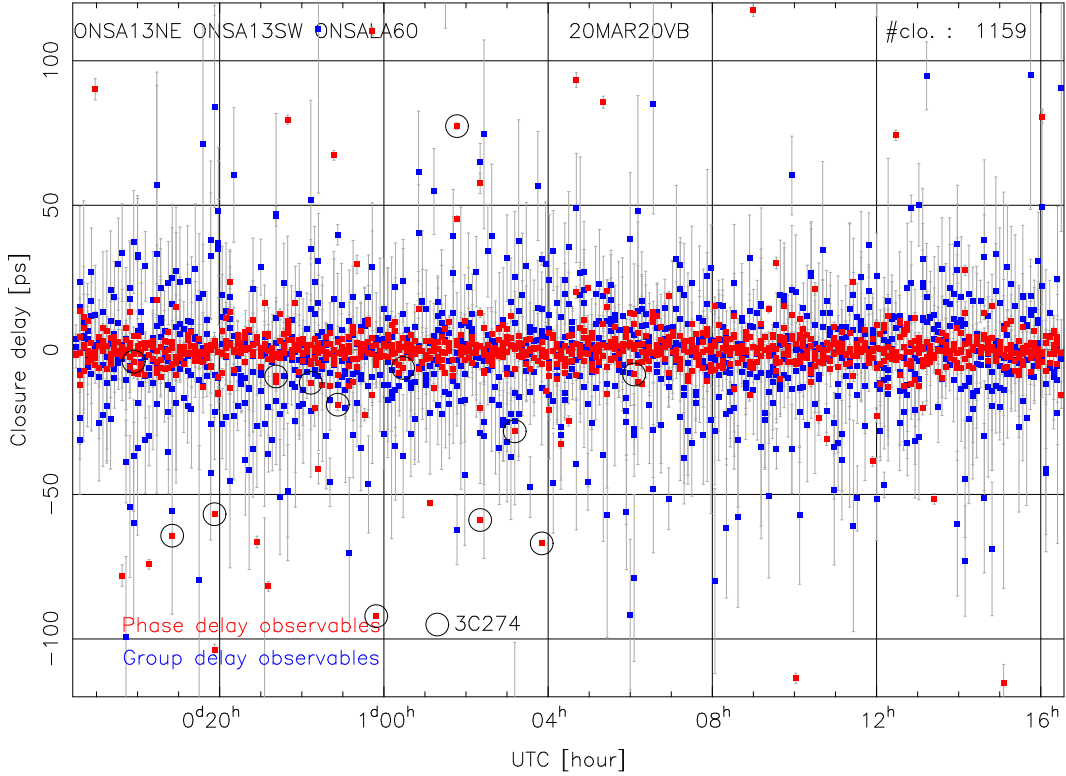


Figure 3. Comparison of closure group delays (blue squares) and closure phase delays (red squares) for the triangle ONSA13NE–ONSA13SW–ONSA1A60 in session ON0080 demonstrates the significantly higher precision of the phase delays than the group delays. The scatter of the closures indicates the contributions of thermal noise. The red squares marked by black circles indicate the observations of source 3C274, which is well known to have large scale structure and has a similar pattern in its closure phases from the other ONTIE sessions with these three antennas. The closures suggest that about 2% of the short-baseline observations may be significantly affected by source structure at large angular scales.

2.5 Data analysis

In the multiple steps of VLBI data processing (see <https://ivscc.gsfc.nasa.gov/about/resolutions/IVS-Res-2019-02-AnalysisLevels.pdf>), geodetic analysis is performed with the aim of estimating the parameters of geodetic interests, such as Earth orientation parameters (EOP), station positions, and source positions. In the geodetic solutions of short-baseline observations, there are two other possible kinds of parameters in addition to baseline vectors: clocks, accounting for the relative behaviors of the two frequency standards and for the instrumental delays, and differential zenith wet delays (dZWDs), accounting for the different atmospheric effects between the two antennas. The clocks were characterized by a continuous piece-wise linear (PWL) function with a time interval of usually one hour (but see the supporting information for additional discussion). For the atmospheric delays, the hydrostatic part was modeled, while the impact of the wet path delays due to water vapour was investigated by comparing the results of the baseline vector estimates from not estimating dZWDs and estimating them using PWL functions of different time intervals. Geodetic analysis was carried out by using either phase delays or group delays.

The software package *ν Solve* (open source, available at <https://sourceforge.net/projects/nusolve/>) was used for the geodetic analyses. For each session, we reset the configuration in the original databases to remove the flagging and weighting information and the ionospheric corrections, excluded the observations of all antennas apart from the two antennas of the desired short baseline in a session, restored all the usable observables, examined and adjusted the phase ambiguities in a program developed by ourselves, flagged the outliers, and performed the solution based on either group delays or phase delays at X band. In geodetic solutions as guided by the *ν Solve* user manual, one step that is commonly used is to determine a baseline-dependent uncertainty in addition to the formal error of each observable in order to derive a more realistic error used for the weighting; this additive uncertainty σ_{add} is a constant value in a session for each baseline and is determined in an iterative way until the reduced χ^2 is unity.

3 Results

When there are more than three sessions available for a baseline, the baseline vector repeatability is defined as the weighted root-mean-square (WRMS) scatter of the relative position estimates from these multiple sessions about the weighted mean value. We evaluated this metric for the three components of a baseline vector and present the results always in the sequence of the east, north, and up directions.

3.1 Baselines with more than two global sessions

3.1.1 WETTZ13N–WETTZELL

Geodetic/astrometric VLBI makes routine observations of tens of radio sources typically for 24 hours or for one hour in one session. These two antennas have simultaneously participated in these two types of IVS observations since 2015 (Schüler et al., 2015).

The correlator centers for processing VLBI observations by using the fringe fitting program *fourfit* started to apply a special mask called *notch* filter to mitigate the corruption due to specific phase calibration signals after October 2018. The width of such a notch filter depends on the spectral resolution which is used for correlation: the higher the resolution, the narrower the notch filters. Therefore, only the sessions since R4889 (April 11, 2019) or processed by the correlators after May 01, 2019 have usable observables on baseline WETTZ13N–WETTZELL. There are 107 sessions as listed in

331 Table S1 in the supporting information. (We note that reprocessing the observations
 332 of this baseline since 2015 from visibility data will produce four more years of usable
 333 observations.) The results from the analyses of not estimating dZWDs for this baseline
 334 are presented here, whereas the results of estimating them will be discussed in Sect.
 335 5. The mean number of total observations in these 107 sessions is 302, and the mean
 336 number of used observables in the solutions is 276 and 277 for group delay analyses
 337 and phase delay analyses, respectively. The mean value of the WRMS delay residuals
 338 is 15.6 ps for group delay analyses and 3.9 ps for phase delay analyses. They are
 339 approximately at the same level as those determined by the closures of the triangle
 340 formed by the Onsala antennas.

341 The mean formal errors of the estimates of the baseline vector in the east, north,
 342 and up directions are 0.6, 0.6, and 1.3 mm from group delay observables, respectively,
 343 and they are 0.2, 0.1, and 0.3 mm from phase delay observables. Because the estimates
 344 from different sessions are scattered more than one would expect from their formal er-
 345 rors, the formal errors were inflated by introducing a constant additive uncertainty
 346 such that the reduced χ^2 of the time series of each coordinate component becomes
 347 unity. The additive uncertainty is an indication of the systematic error level in the re-
 348 sults that is not measured by the (original) formal error. They are 0.8, 2.5, and 2.3 mm
 349 for the three position components from group delay analyses, and 0.3, 0.3, and 0.7 mm
 350 for phase delay analyses, respectively. The results suggest that the sub-millimeter
 351 accuracy can be achieved for all the three components of this short baseline by phase
 352 delays in a single 24-hour session with the S/X observing mode.

353 We used the inverse of the sum of the squares of the formal error and the additive
 354 uncertainty as the relative weight for each individual estimate from one session in
 355 calculating the weighted mean baseline vector and the repeatability. The weighted
 356 mean of the baseline vector estimates from both group delays and phase delays are
 357 presented in Table 2. The baseline vector repeatabilities are 0.3, 0.3, and 0.8 mm from
 358 phase delay analyses and 1.1, 2.6, and 3.0 mm from group delay analyses. The precision
 359 obtained for this 123 m baseline based on phase delays is likely to demonstrate the best
 360 performance that the geodetic VLBI system with the S/X observing mode is capable
 361 of. The repeatabilities of the position of WETTZELL based on group delays in the 24-
 362 hour global sessions are 3, 5, and 9 mm according to the IVS internal report of the
 363 ITRF2020 on the 20th IVS analysis workshop in September 13, 2021.

364 The residuals of the baseline vector estimates from both phase delays and group
 365 delays are shown in Fig. 4. There is a significant difference in the up direction between
 366 group delay and phase delay results; the weighted mean of the up estimates from group
 367 delays is lower than that from phase delays by 1.7 ± 0.2 mm. The distribution of the
 368 residuals in the horizontal plane is shown in Fig. 5. The majority of the east and north
 369 residuals from the phase delay analyses are within ± 0.5 mm. The residuals from group
 370 delay analyses systematically spread in the north direction, but they do not show a
 371 temporal dependence. The results from group delays in the 24-hour global sessions
 372 also have a larger scatter in the north direction than in the east direction as shown
 373 in the IVS internal report of the ITRF2020. The differences in the mean horizontal
 374 components between group delay results and phase delay results are within three times
 375 the uncertainties of the group delay results.

376 Complementary to the 24-hour sessions, Intensive sessions have been carried out
 377 since 1984 (Robertson et al., 1985) to rapidly determine Earth’s highly variable phase
 378 of rotation. They last for one hour and currently are observed every day by two globally
 379 spaced antennas, generally WETTZELL and KOKEE, and every Monday by more than two
 380 antennas including WETTZELL and WETT13N. Due to continuous improvements in VLBI
 381 antenna sensitivities and in scheduling (see, e.g., Baver & Gipson, 2020; Schartner et
 382 al., 2021), and taking advantage of the consequent more even distribution of usable
 383 radio sources on the sky, it has become possible to estimate relative positions for the co-

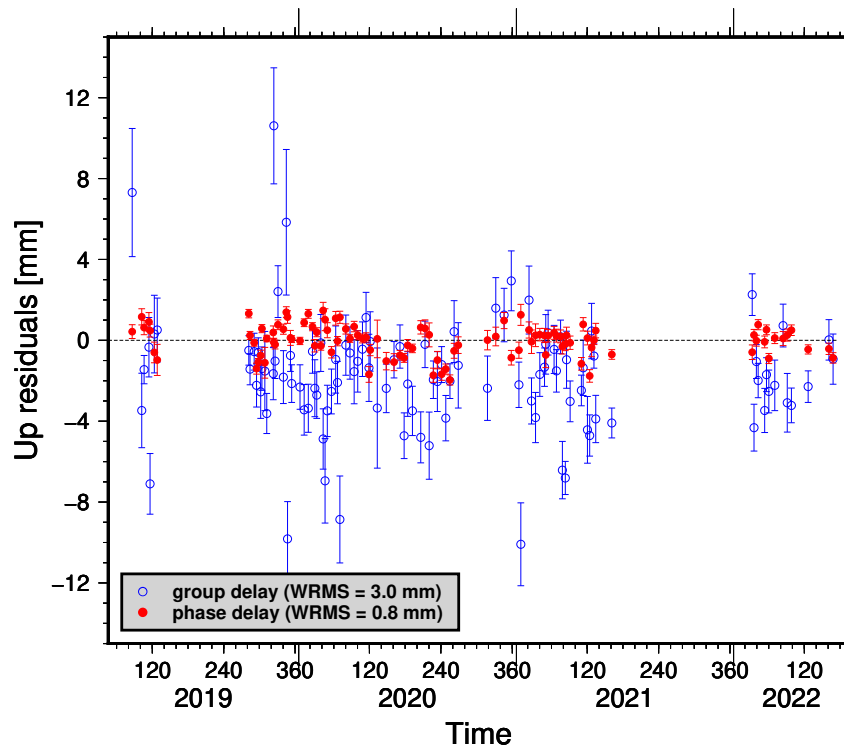


Figure 4. Residuals of the estimated up coordinates of baseline vector WETTZ13N–WETTZELL from group delay observables (blue open circles) and phase delay observables (red closed circles) based on geodetic analyses of 107 global 24-hour sessions. The error bars are the formal errors of the estimates from geodetic analyses.

Table 2. Weighted mean estimates of the baseline vectors, in geocentric (XYZ) and topographic (ENU) coordinate systems, for the four baselines that have data of more than two VLBI sessions (units: mm). The topographic coordinate system in this work is defined to be centered at the position of the first antenna of a baseline. The baseline vector WETT13N–WETT2ELL from local survey is reported for comparison. L is baseline length with uncertainty σ_L .

Baseline	Observable	X	σ_X	Y	σ_Y	Z	σ_Z	L^1	σ_L
Wn–Wz	Group delay	−88034.29	0.26	−38730.62	0.08	77165.27	0.26	123306.83	0.24
	Phase delay	−88035.64	0.06	−38730.82	0.03	77164.15	0.05	123307.14	0.03
	Local survey	−88036.3	0.49	−38731.5	0.47	77162.8	0.52	123307.0	0.50
Ns–Ny	Group delay	1391812.79	0.88	605228.09	0.50	−256274.30	3.81	1539193.64	0.41
	Phase delay	1391815.79	0.28	605228.50	0.28	−256258.16	1.15	1539193.54	0.21
Is–Ts	Group delay	2226595.94	0.84	13403264.28	0.56	−9547965.53	0.94	16606290.08	0.53
	Phase delay	2226601.17	0.56	13403259.09	0.44	−9547970.00	0.55	16606289.11	0.24
Hh–Ht	Group delay	48041.29	0.86	−102300.32	0.59	4125.36	0.66	113094.39	0.53
	Phase delay	48042.17	0.63	−102300.89	0.18	4126.25	0.63	113095.28	0.30
		E	σ_E	N	σ_N	U	σ_U		
Wn–Wz	Group delay	−18136.24	0.10	121917.55	0.25	−3422.47	0.27		
	Phase delay	−18136.08	0.03	121918.05	0.03	−3424.22	0.08		
	Local survey	−18136.6	0.47	121917.8	0.50	−3425.8	0.51		
Ns–Ny	Group delay	306380.24	0.48	−1508019.93	0.44	33575.12	3.84		
	Phase delay	306380.05	0.30	−1508019.81	0.26	33591.55	1.14		
Is–Ts	Group delay	−11725044.07	0.31	−11759335.74	0.50	−101167.29	1.24		
	Phase delay	−11725043.48	0.21	−11759334.70	0.23	−101175.48	0.84		
Hh–Ht	Group delay	−112908.81	0.53	1532.81	0.50	−6289.81	1.02		
	Phase delay	−112909.85	0.33	1533.84	0.44	−6289.73	0.74		

¹ Baseline length L is derived as the mean of the baseline length estimates over multiple sessions in the same way as for the three position components; therefore, there can be a discrepancy of a few tenths of millimeter between the reported L and the value that one can calculate from the root of the sum of the squares of the three position components. Uncertainty σ_L is calculated from the time series of the baseline length estimates as the uncertainty of the mean value instead of doing error propagation from the uncertainties of the three position components. This process provides an evaluation of baseline length as an independent quantity and is used in the study for these four baselines.

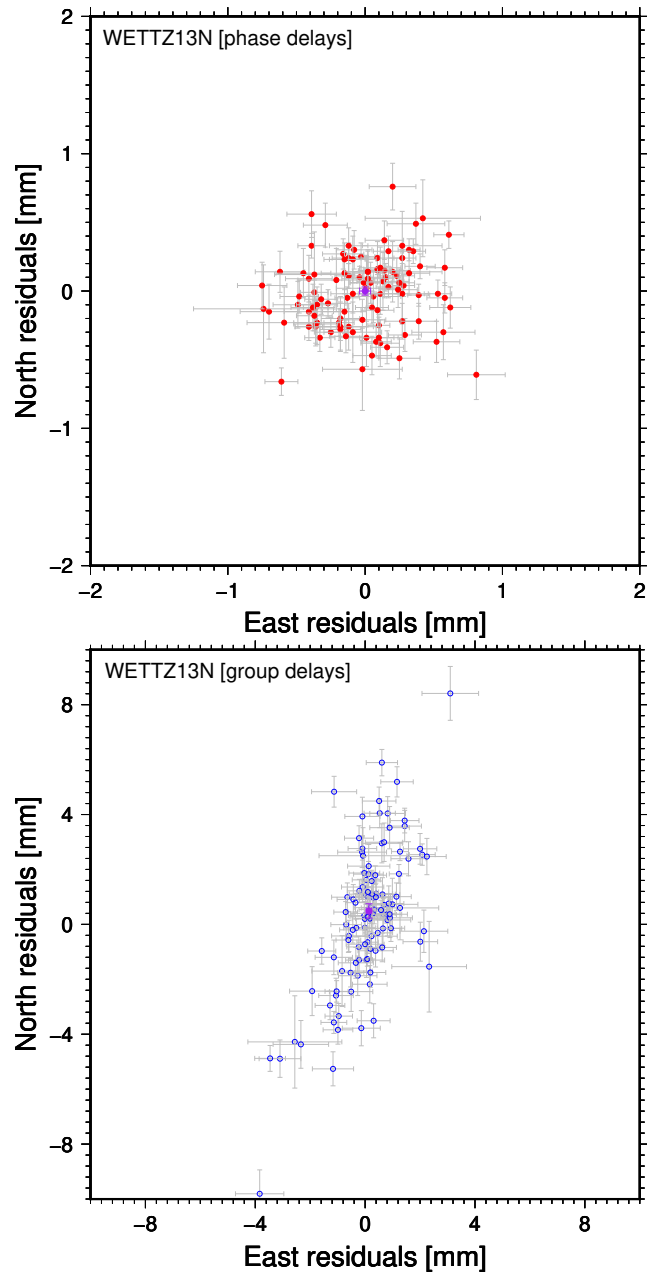


Figure 5. Residuals of the position estimates of baseline WETT13N–WETT2ELL in the horizontal plane from group delays (bottom) and phase delays (top) in the 107 global 24-hour sessions. The residuals in both plots are relative to the weighted mean position from phase delays. The weighted mean of the residuals is marked as a purple dot in both plots. Note the different scale.

384 located pair WETTZELL and WETTZ13N from the Intensive sessions. We use the Intensive
 385 sessions here to learn how well the short baseline vector can be determined from one-
 386 hour observations by comparing to the results obtained from 24-hour observations.

387 We have processed 58 Intensive sessions that included the WETTZ13N–WETTZELL
 388 baseline within the same time period as the 24-hour sessions, listed in Table S2 in the
 389 supporting information. These Intensive sessions on average consist of 43 scans, and
 390 the mean number of usable observables of the baseline is 39.0 and 39.6 for group delay
 391 and phase delay, respectively. They are at least twice the average numbers per hour of
 392 24-hour sessions. In the data analysis of the Intensive only six parameters are set up:
 393 three for the baseline vector and three for the clock. The means of the WRMS delay
 394 residuals are 9.5 ps for group delay analyses and 3.1 ps for phase delay analyses, which
 395 are significantly smaller than those of the solutions based on the 24-hour sessions.
 396 However, since the Intensive sessions do not have significantly higher signal to noise
 397 ratio than the regular IVS global 24-hour sessions, these smaller delay residuals in the
 398 Intensive sessions may indicate that the shorter sessions are over-parameterized.

399 The residuals of the position estimates from the Intensives with respect to the
 400 reference position obtained from 24-hour sessions are shown in Fig. 6. The mean of the
 401 residuals from phase delays is -0.19 ± 0.16 mm, -0.23 ± 0.14 mm, and 0.20 ± 0.17 mm in
 402 the east, north, and up directions, respectively; they are 0.07 ± 0.44 mm, -0.19 ± 0.51 mm,
 403 and 0.71 ± 0.60 mm for group delays. The formal errors of the position estimates based
 404 on phase delays are on the level of 0.6, 0.6, and 0.8 mm for the three components, re-
 405 spectively; the additive uncertainties to these formal errors are 1.0, 0.8, and 1.0 mm in
 406 order to get the χ^2 of the residual time series being unity. The differences in the
 407 mean positions between the one-hour observations and the 24-hour observations are
 408 not significant with respect to their uncertainties. However, the position residuals show
 409 systematic variations, mainly in southwest and northeast as shown in Fig. 6. The phase
 410 delay analyses produce a baseline vector repeatability of 1.3, 1.1, and 1.3 mm, and the
 411 group delay analyses result in 3.4, 4.0, and 4.5 mm. Phase delays on a short baseline
 412 in an Intensive session have a capability of determining baseline vectors at the 1 mm
 413 level.

414 3.1.2 NYALE13S–NYALES20

415 The legacy antenna NYALES20 in Norway has an observing history of about
 416 30 years, and it is still one of the most active geodetic stations. The new antenna
 417 NYALE13S has participated in the IVS sessions since early 2020 and operated through
 418 a series of shakedown experiments; the legacy antenna NYALES20 observed many ses-
 419 sions in 2020 and 2021 with a warm receiver. Thus, the observations of this baseline
 420 often have large noise contributions. Due to the large measurement noise and the poor
 421 a priori position of the new antenna, it can be challenging to eliminate the phase am-
 422 biguities for this baseline. We have 19 sessions available for this baseline to perform
 423 both phase delay and group delay analyses. The atmospheric effects were modeled
 424 as a PWL function with an interval of one hour in the data analyses of this 1.5 km
 425 baseline. The number of the used observables and the WRMS delay residuals based on
 426 two types of observables are reported in Table S3 in the supporting information. The
 427 mean of the WRMS delay residuals from the IVS reports of the routine data analysis,
 428 labeled as ‘S/X band delays’ in the table, is 53 ps for on average 220 used observables,
 429 and the residuals are significantly larger than the typical measurement noise level in
 430 the geodetic observations. By removing the involvement of the S band observables in
 431 the analyses, labeled as ‘Group delays’ in the table, the number of usable observables
 432 increased by 34%, and the mean of the WRMS delay residuals decreased to 35 ps. A
 433 significant improvement has been obtained by using group delays at X band. The
 434 mean of the WRMS phase delay residuals is about 16 ps, a significant decrease from
 435 the group delay value.

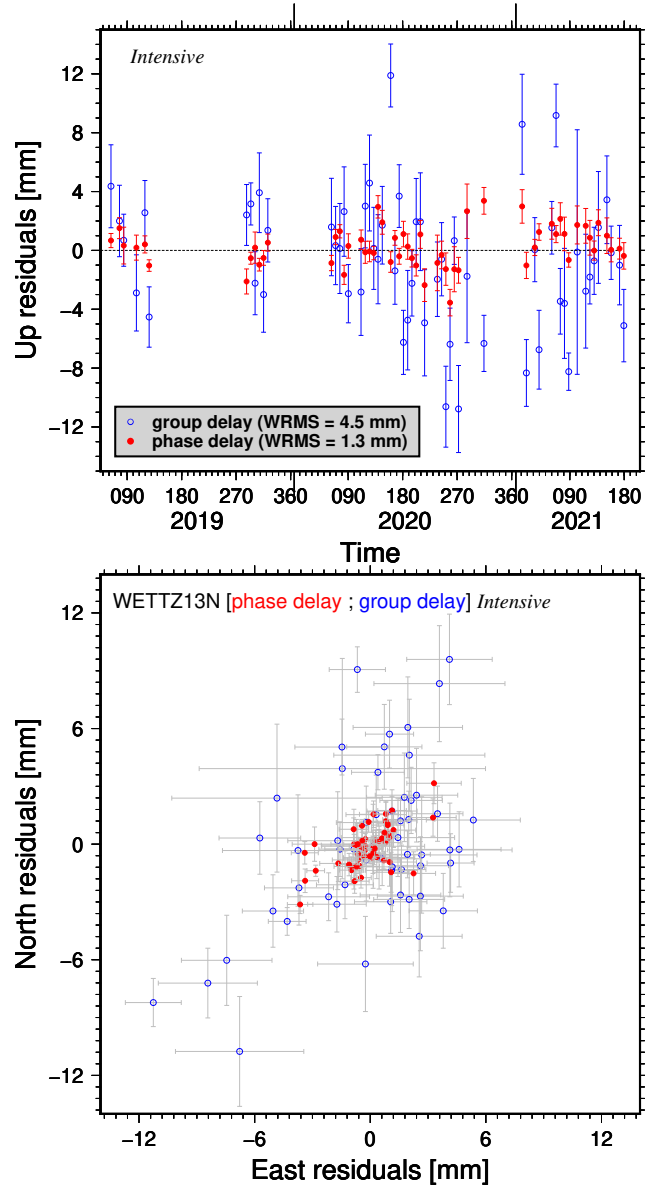


Figure 6. Residuals of the up component (top) and the east and north components (bottom) of baseline vector WETTZ13N–WETTZELL estimates from 58 Intensive sessions, relative to the weighted mean position from phase delays in 24-hour sessions reported in Table 2. Note the different scale compared to the residual scatter shown in Fig. 5.

436 The weighted mean estimate of the baseline vector calculated as the mean esti-
 437 mate is reported in Table 2. The phase delay results yield a baseline vector repeatability
 438 of 1.3, 1.1, and 4.7 mm, and the group delay analyses yield 2.0, 1.8, and 16.0 mm. The
 439 repeatability determined by group delays in the up direction is one order of magnitude
 440 larger than that in the horizontal directions, which means that either the large noise
 441 level in group delays has a larger impact on the up direction or the large noise in the
 442 group delays are not purely random but includes some systematic errors. As the group
 443 delays of this baseline obtained based on manual phase calibration have a significantly
 444 lower noise level than those based on phase calibration signals, the issues in the group
 445 delay results may be due to the phase calibration systems. Referring to the mean
 446 position from phase delays, the residuals are shown in Fig. 7 for both phase delays and
 447 group delays. The difference between the mean estimates from group delay analyses
 448 and phase delay analyses is within the uncertainties of the group delay results in the
 449 horizontal plane and about four times the uncertainty in the up direction.

450 3.1.3 *ISHIOKA–TSUKUB32*

451 The new antenna *ISHIOKA* can observe with both the S/X and the VGOS mode,
 452 thanks to the interchangeable S/X band and broadband receivers. The 32 m antenna
 453 *TSUKUB32* ended observing in December 2016, and it was dismantled in 2017. It is
 454 only possible to derive the position tie for this 16.6 km baseline by analyzing historical
 455 observations. The reported results of this baseline are from estimating the dZWDs
 456 with an interval of one hour. The phase delays in the 17 sessions listed in Table S4
 457 in the supporting information produce a baseline vector repeatability of 0.9, 0.9, and
 458 3.4 mm, and the group delays give 1.2, 2.0, and 4.7 mm. The reference position and the
 459 mean position from group delay analyses are listed in Table 2. The difference between
 460 the group delay and phase delay results is 8.2 mm in the up direction, significant at
 461 the 5-sigma level, and is about 1 mm in the horizontal plane.

462 3.1.4 *HARTRAO–HART15M*

463 Because the frequency standard of antenna *HART15M* was tuned down by ~ 4.5 Hz,
 464 this short baseline has usable observables without applying the notch filter in correla-
 465 tion. The solutions based on the phase delays of this baseline are only slightly better
 466 than the ones based on group delays as indicated by the WRMS delay residuals in
 467 Table S5 in the supporting information. The mean estimates of the baseline vector
 468 from phase delays and group delays in the eight sessions are presented in Table 2. The
 469 differences between the results from the two types of observables are not significant
 470 with respect to their uncertainties.

471 3.2 Baselines with only one or two global sessions

472 The results of the baseline vectors from phase delays for the baselines with only
 473 one or two global sessions available are reported in Table 3. The VLBI data for the
 474 baseline *SESHAN13–SESHAN25* are from session AOV056 (February 03, 2021), and the
 475 data for the other six baselines are from two mixed sessions, RD2005 (June 24, 2020)
 476 and RD2006 (July 08, 2020). The detail of the data analysis of these observations are
 477 presented in the supporting information.

478 4 Comparison of the results

479 Local survey measurements have been carried out at the Wettzell site to obtain
 480 the baseline vectors with an uncertainty of about 0.5 mm in each of the three compo-
 481 nents. The local-survey result of the baseline vector *WETTZ13N–WETTZELL* is reported
 482 in Table 2. This result was derived from the local tie measurements over the course

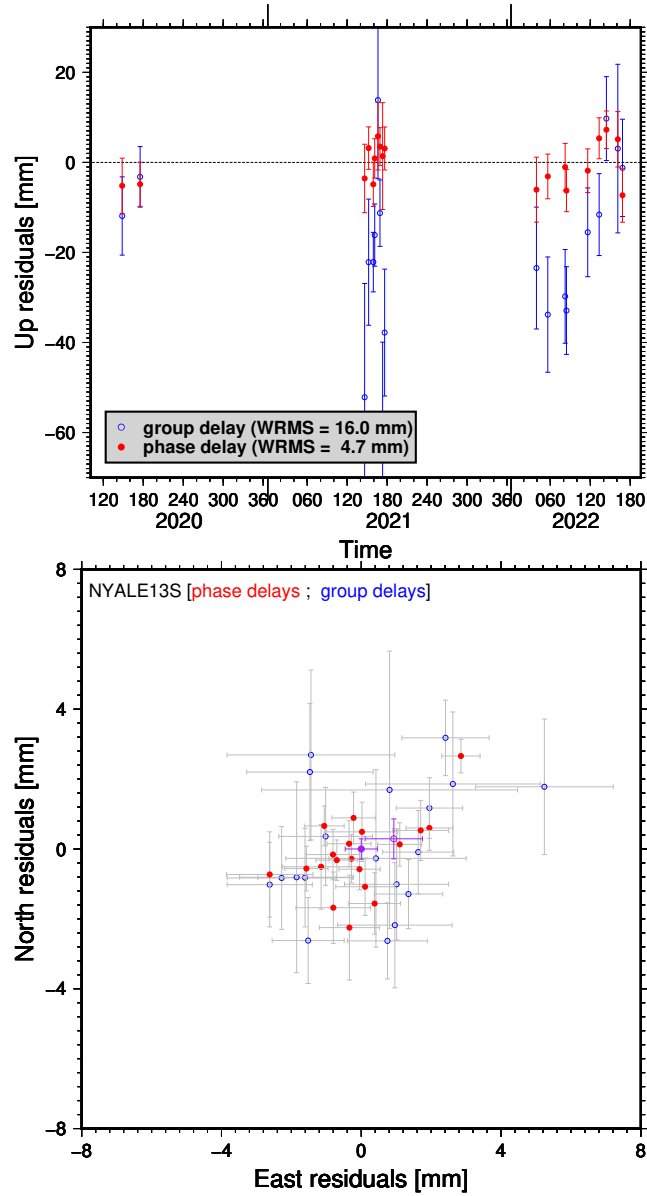


Figure 7. Residuals of the Up component (top) and the east and north components (bottom) of baseline vector NYALE13S–NYALES20. The residuals are drawn by blue open circles for group delay results, and by red closed circles for phase delay results. The weighted means of the residuals are marked as purple dots in the bottom plot.

Table 3. Estimates of the baseline vectors, in geocentric (XYZ) and topographic (ENU) coordinate systems, for the seven baselines that have only one or two VLBI sessions (units: mm). L is baseline length with uncertainty σ_L . The results are from geodetic solutions based on phase delays. The baseline vector WETT13S–WETT2ELL determined from the local survey measurements is reported.

Baseline	Session	X	σ_X	Y	σ_Y	Z	σ_Z	L	σ_L
S6–Sh	AOV056	−40596.42	0.58	3901.92	0.51	−37658.70	0.45	55511.01	0.42
Ws–Wz	RD2005	−119342.49	0.28	−89237.27	0.18	113297.05	0.32	187195.46	0.18
	RD2006	−119345.03	0.34	−89238.05	0.22	113293.70	0.41	187195.43	0.22
	Local survey	−119344.4	0.41	−89236.0	0.38	113294.3	0.43	187194.4	0.41
Yj–Ys	RD2005	−69291.94	0.54	145344.50	0.33	108556.53	0.55	194192.99	0.35
K2–Kk	RD2006	−6068.11	0.23	19214.95	0.17	23720.61	0.17	31124.00	0.14
On–Ow	RD2005	340935.36	0.20	−383169.93	0.16	−169947.25	0.25	540313.04	0.16
	RD2006	340935.31	0.23	−383170.17	0.15	−169947.31	0.31	540313.20	0.17
Oe–On	RD2005	−283454.24	0.19	346477.62	0.16	138824.67	0.25	468684.69	0.15
Oe–Ow	RD2005	57480.67	0.09	−36692.52	0.07	−31123.37	0.13	74960.20	0.07
		E	σ_E	N	σ_N	U	σ_U		
S6–Sh	AOV056	32703.72	0.30	−44832.37	0.39	1413.22	0.65		
Ws–Wz	RD2005	−60393.44	0.17	177152.60	0.18	−3424.98	0.39		
	RD2006	−60393.63	0.22	177152.42	0.23	−3429.24	0.48		
	Local survey	−60391.8	0.38	−177152.0	0.42	−3428.1	0.42		
Yj–Ys	RD2005	141400.02	0.33	132564.10	0.32	11987.94	0.70		
K2–Kk	RD2006	−20126.13	0.14	22345.63	0.12	8019.67	0.28		
On–Ow	RD2005	−445354.61	0.12	−305876.39	0.12	−6091.16	0.26		
	RD2006	−445354.81	0.16	−305876.33	0.15	−6091.27	0.36		
Oe–On	RD2005	397551.87	0.12	248155.52	0.12	6057.04	0.26		
Oe–Ow	RD2005	−47773.49	0.07	−57764.40	0.07	4.55	0.15		

of several years, and thus has no nominal temperature of the local environment. Nevertheless, as we will see in section 5, the baseline vectors among the antennas at the Wettzell site are very insensitive to the thermal expansion on the three antennas. The difference of the baseline vector from phase delays with respect to the local survey is 0.5, 0.3, and 1.6 mm in the east, north, and up directions, respectively, and it is 0.4, 0.2, and 3.3 mm for group delays. The VLBI results do not significantly differ from the local-survey tie in the horizontal directions, but the differences in the up direction are significant. The up component from phase delays is closer to the local survey than from group delays for this baseline. As reported in Table 3, the local-survey tie of another short baseline at Wettzell, WETTZ13S–WETTZELL, has a significant difference (at the $3\text{-}\sigma$ level) in the east direction with respect to the VLBI results, about 1.5 mm. For the 4.3 mm difference in the Up component between the results from the two sessions RD2005 and RD2006, the local survey shows a better consistence with the RD2006 result. The comparisons of these two baselines suggest that the VLBI results and the local survey measurements may have a difference of 1–2 mm in the horizontal directions and up to a few mm in the Up direction.

As mentioned, the results of the short baselines at the Kokee Park and at the Onsala Space Observatory were previously reported by Niell et al. (2021) and Varenius et al. (2021), respectively. Compared with the result of the baseline KOKEE12M–KOKEE from VLBI measurements with an mean date of April 11, 2016 (Niell et al., 2021), the change of our result is insignificant in the horizontal directions but has a magnitude of 4.0 mm in the Up direction. For the legacy antenna and the twin VGOS antennas at the Onsala Space Observatory, the difference in the baseline vector ONSA13NE–ONSA13SW between our results and that reported in Varenius et al. (2021) is less than 0.2 mm in the horizontal directions and 0.8 mm in the Up direction.

As an independent determination of the baseline vectors at the accuracy of the sub-mm level, our results from phase delays were used to validate the latest realization of ITRF, ITRF2020 (see <https://itrf.ign.fr/en/solutions/ITRF2020>). See Table 4. There are two baselines not listed in the table: ISHIOKA–TSUKUB32 because of the post-seismic deformation model employed for station TSUKUB32 in the ITRF2020 but not for station ISHIOKA and SESHAN13–SESHAN25 due to the missing station SESHAN13 in the ITRF2020. The listed nine baselines all have the position differences larger than 1 mm, even though most of them are consistent with the uncertainties that are dominated by that of the ITRF2020. Two baselines have the differences at the cm level: NYALE13S–NYALES20 and RAEGYEB–YEBES40M. The former baseline vector has only been determined with an accuracy of several centimeters in the ITRF2020 due to the large impact from S band as discussed in sections 2.4 and 3.1.2, and the latter one is most likely affected by the receiver replacement at YEBES40M in 2011.

5 Discussion on sources of error

It is worthwhile to note that sub-millimeter repeatability has been demonstrated through short baselines by other space geodetic techniques than VLBI, for instance, the Global Navigation Satellite Systems (GNSS) by Hill et al. (2009); King & Williams (2009). These studies have used the short-baseline time series to investigate the site-specific errors and the stability for GNSS. However, due to completely different data collection and processing methods between the various space geodetic techniques, the sub-millimeter repeatability and the error investigation should be carried out independently for each technique toward the 1 mm accuracy goal of global geodesy.

An early phase delay analysis of eleven VLBI sessions of the 1 km baseline HAYSTACK–WESTFORD determined a baseline vector repeatability of 5, 3, and 7 mm in the east, north, and up components (Carter et al., 1980). Then, later with the improved Mark III VLBI system, Herring (1992) obtained a repeatability of 0.8, 0.7, and 2.3 mm

Table 4. Differences of the baseline vector estimates from short-baseline phase delays with respect to the ITRF2020, which are listed in Table S6 in the supporting information (units: mm).

Baseline	Monument	Observable	X	σ_X	Y	σ_Y	Z	σ_Z
Wn–Wz	7387–7224		0.86	1.28	1.08	1.20	1.25	1.50
Ns–Ny	7392–7331		–7.61	25.21	12.50	25.31	5.34	27.44
Hh–Ht	7378–7232		6.37	2.08	1.91	1.64	–2.85	1.94
Ws–Wz	7388–7224	RD2005	0.81	1.63	0.93	1.45	2.25	1.87
		RD2006	–1.73	1.65	0.15	1.46	–1.10	1.89
Yj–Ys	7389–7386	RD2005	26.76	2.36	–0.30	1.54	25.63	2.36
K2–Kk	7623–7298	RD2006	7.79	3.90	–3.55	2.97	–2.09	3.45
On–Ow	7213–7637	RD2005	1.06	2.95	–0.43	1.98	–1.35	4.52
		RD2006	1.01	2.95	–0.67	1.98	–1.41	4.52
Oe–On	7636–7213	RD2005	1.26	2.48	0.42	1.80	4.47	3.55
Oe–Ow	7636–7637	RD2005	1.87	3.62	–0.22	2.41	2.33	5.56

534 for the same baseline by using phase delays in 24 VLBI sessions. The baseline length
535 of WETTZ13N–WETTZELL is 123 m, one order of magnitude shorter than that of baseline
536 HAYSTACK–WESTFORD; both baselines observed in the S/X mode. As a continuation
537 of the investigations from six sessions of WETTZ13N–WETTZELL in [Halsig et al. \(2019\)](#),
538 which were based on group delays, the larger dataset of 107 global 24-hour sessions and
539 58 Intensives over 2.5 years and the significantly improved repeatability in our study
540 provide the opportunity to assess the error components more stringently.

541 What are the important sources of error in the repeatability of the baseline vector
542 estimates of this short baseline? The investigation based on the metric of repeatability
543 in most cases is sufficient for geophysical and astrophysical studies, such as a change
544 in the orientation of the Earth in space and the station position variations due to tidal
545 displacements or tectonic motions. However, some of the instrumental effects can be
546 highly repeatable and thus are not detected by the WRMS scatter of the estimates.
547 It is necessary to also investigate those repeatable errors in the VLBI system itself for
548 the purpose of combining the station positions from various space techniques for the
549 realization of ITRF. Therefore, which of these error components are repeatable (related
550 to accuracy) or not repeatable (precision)? We devote this section to addressing these
551 questions.

552 (1) *Measurement noise in delay observables* The uncertainty of a baseline vector
553 estimate due to measurement noise in observables generally manifests itself as the
554 formal error from the geodetic solution based on least square fitting (LSF). A session-
555 wise delay noise was added in quadrature to the uncertainties of the observables in
556 LSF to account for potential systematic errors already at the observation level. And
557 in fact, the additive noise is comparable to the corresponding WRMS delay residual
558 as shown in Table S2 in the supporting information. Therefore, the uncertainty due
559 to measurement noise is lower than the formal error of the estimate by a factor of
560 approximately $\sqrt{2}$. Taking this factor into account, the impact of measurement noise in

561 phase delays on the baseline vector of WETTZ13N–WETTZELL is 0.1 mm on the horizontal
 562 plane and 0.4 mm in the up direction, and for group delays it is 0.5 mm and 2.0 mm.

563 (2) *Cable delays* The time delays of the astronomical signal passing through the
 564 electronic devices within the antennas are expected to be smoothly varying and are ab-
 565 sorbed in the clock parameters. In order to eliminate their variations, phase calibration
 566 systems are used to correct the visibility phases. Meanwhile, the time delays through
 567 the cable that carries the precisely timed pulses from the frequency standard to the
 568 injection of phase calibration signals are actually not experienced by the astronomical
 569 signals; these cable delays are measured as corrections to be applied in geodetic solu-
 570 tions. Of the eleven baselines in this study, only KOKEE12M–KOKEE, RAEGYEB–YEBES40M,
 571 WETTZ13S–WETTZELL, and the baselines formed by the Onsala antennas have the cable
 572 delay corrections available for both antennas. In fact, proxy corrections for KOKEE12M
 573 instead of direct measurements were used (see, Niell et al., 2021), and the cable delay
 574 corrections of antenna RAEGYEB were not applied for the final solution. It is possi-
 575 ble that variations of the time delays in the antenna electronics and cabling cause
 576 significant impacts due to the missing corrections for some antennas.

577 We ran geodetic solutions of the 107 sessions in which the cable delay corrections
 578 of antenna WETTZELL were not applied by intention. We must emphasize that turning
 579 off the cable delay corrections did not degrade the solutions in the sense of the WRMS
 580 delay residuals and the baseline vector repeatability when comparing to the solutions
 581 with the corrections applied. After turning off the cable delay corrections of antenna
 582 WETTZELL, the mean of the changes in the baseline vector estimates from phase delays is
 583 0.23 ± 0.03 mm, 0.07 ± 0.02 mm, and 1.65 ± 0.11 mm in the east, north, and up directions,
 584 respectively. As discussed in the supporting information, the cable delay corrections of
 585 antenna RAEGYEB have an impact of about 6 mm on the up direction. For the ONSALA60
 586 antenna, the impact is estimated to be dominant also in the up direction, which is even
 587 at the level of 1 cm (Varenius et al., 2021). The uncertainty due to missing cable delay
 588 calibrations may be at the sub-millimeter level on the horizontal directions and a few
 589 millimeters or larger in the up direction. The impact is repeatable at the 0.1 mm
 590 level for antenna WETTZELL. This repeatable feature may affect other antennas if the
 591 distribution of the elevation and azimuth angles does not change dramatically from
 592 session to session such that the cable is twisted in the same manner.

593 (3) *Antenna thermal expansion* The antenna structure experiences thermal defor-
 594 mation, and this leads to station position changes due to the temperature variations at
 595 the site. This effect and the models have been well studied (see, e.g., Nothnagel, 2009,
 596 and the references therein). The antenna-dependent parameters in these models are
 597 maintained and publicly available for most of the geodetic antennas (from [https://raw](https://raw.githubusercontent.com/anothnagel/antenna-info/master/antenna-info.txt)
 598 [.githubusercontent.com/anothnagel/antenna-info/master/antenna-info.txt](https://raw.githubusercontent.com/anothnagel/antenna-info/master/antenna-info.txt)).
 599 However, the practical problem of applying these models at the observation level in
 600 geodetic solutions can be that the desired temperatures of the antenna structural ele-
 601 ments are specific functions of the time history of the ambient temperatures. Therefore,
 602 the information of these temperatures are not complete in VLBI databases. Neverthe-
 603 less, the mean temperature during the 24 hours of observations would not significantly
 604 differ from the mean value of the temperatures that actually cause the thermal ex-
 605 pansion. We use the temperatures recorded at the same epochs of observations in a
 606 session to derive the mean value and assess this source of error accordingly.

607 The temperature dependence of antenna thermal expansion consists of constant
 608 terms and elevation-dependent terms. In the case of WETTZ13N and WETTZELL, which
 609 have zero axis offsets, the elevation-dependent terms are proportional to the sine of the
 610 elevation angle. The extra path length due to the thermal expansion mimics exactly
 611 the effect of a vertical displacement of the antenna. The relative foundation height of
 612 WETTZ13N minus WETTZELL is -2 m with an expansion coefficient of 1.0×10^{-5} per $^{\circ}\text{C}$,
 613 and the relative height of the supporting axes is $+1$ m with an expansion coefficient of

614 1.2×10^{-5} per $^{\circ}\text{C}$. Therefore, an increase of 1°C at the site will cause the up component
 615 of WETTZ13N’s position (relative to WETTZELL) to decrease by 0.008 mm. Based on
 616 the meteorological data recorded at each observation epoch, the median value of the
 617 mean temperatures in these sessions is 7.7°C , which is very close to the reference
 618 temperature of the model parameters previously mentioned. The rms scatter of the
 619 temperatures within one session has a median value of 2.3°C ; thus, the impact due
 620 to the temperature variations within a day is negligible. There is a seasonal variation
 621 in the mean temperatures with an amplitude of $11.5 \pm 0.7^{\circ}\text{C}$. Even though the actual
 622 variations due to this effect will be about -1.4 mm in winter and about $+1.4$ mm
 623 in summer for both antennas, the corresponding impact on the baseline vector of
 624 WETTZ13N–WETTZELL has a magnitude of only 0.1 mm in the up component.

625 For baseline ONSALA60–ONSA13SW from June 24 to July 08, 2020, the impact of
 626 thermal expansion is about 0.2 mm in the up direction due to the temperature change
 627 of 5.2°C at the site. We also note that the temperatures can be different between these
 628 two antennas because ONSALA60 is enclosed in a radome. Nevertheless, the impact of
 629 this effect cannot explain the difference in the estimates of the up component of this
 630 baseline vector from the two sessions, as presented in Table 3. The impact of thermal
 631 expansion is typically very small (i.e., below 1 mm) for the short baselines except
 632 RAEGYEB–YEBES40M, since the temperature is close to the same for multiple antennas
 633 at a site and they tend to have similar physical dimensions. This source of error should
 634 show a seasonal variation in the up direction.

635 (4) *Antenna gravitational deformation* In contrast to the constant, known co-
 636 efficients of thermal expansion, the gravitational deformation of the main reflector
 637 and its distance to the secondary reflector needs to be measured individually for each
 638 antenna. Extensive measurements of this effect for the Onsala antennas have been
 639 made by employing other measuring techniques (see, e.g., Nothnagel et al., 2019;
 640 Bergstrand et al., 2019; Lösler et al., 2019). These studies demonstrated that the
 641 effect produces systematic offsets in the up component of the position of the 20
 642 m Onsala antenna of about 1 cm; however, the change is smaller than 1 mm for
 643 the 13.2 m VGOS antennas at the site. These results may be considered repre-
 644 sentative of the impacts on the legacy antennas and the VGOS antennas at the
 645 other geodetic VLBI sites. The IVS recently adopted the resolution of every radio
 646 telescope operating in IVS observing sessions being surveyed for gravitational de-
 647 formation investigations (see [https://ivscc.gsfc.nasa.gov/about/resolutions/
 648 IVS-Res-2019-01-TelescopeSurveys.pdf](https://ivscc.gsfc.nasa.gov/about/resolutions/IVS-Res-2019-01-TelescopeSurveys.pdf)).

649 The extra raypath introduced by antenna gravitational deformation is a smooth
 650 curve with respect to elevation angle, as measured for ONSALA60, similar to a sine
 651 function. Therefore, the major impact on station position estimates is on the up
 652 component, as shown in the data analysis of Varenius et al. (2021). If this elevation
 653 dependence were exactly a sine function, the impact would again be equivalent to a
 654 displacement in the up position with a magnitude of the gravitational deformation at
 655 zenith direction. Moreover, regardless of whatever is the exact form of the elevation
 656 dependence, the impact on position estimates is repeatable as long as the elevation
 657 angles have a similar distribution from one session to another. This is valid for baseline
 658 WETTZ13N–WETTZELL, because there is no significant difference in the scheduling of the
 659 107 sessions with the same goal — only four of the 107 sessions are for the determina-
 660 tion of TRF and the other 89 are R1 and R4 sessions. Nevertheless, we might conclude
 661 that the non-repeatable component of the antenna gravitational deformation is likely
 662 smaller than the repeatability of the baseline vector WETTZ13N–WETTZELL.

663 Since the gravitational deformation of the VGOS antennas is measured to be
 664 below 1 mm (though to be measured and confirmed for more VGOS antennas), an
 665 order of magnitude smaller than that of the legacy antennas, the corresponding error
 666 for VGOS is expected to be smaller than that of baseline WETTZ13N–WETTZELL.

667 (5) *Antenna tilt* It is possible that the supporting axis of an antenna tilts toward
 668 a direction in the horizontal plane as time goes on (Niell et al., 2021). Based on the
 669 3.5 years of observations of WETTZ13N–WETTZELL, however, the horizontal motion is
 670 determined to be negligible, -0.02 ± 0.04 mm/yr and -0.03 ± 0.03 mm/yr in the east
 671 and north directions, respectively.

672 (6) *Signal chain* Due to the large systematic differences in group delay and phase
 673 delay observables as shown in Fig. 2, we believe that there is a possibility of significant
 674 errors introduced in the signal chain before the injection of phase calibration signals or
 675 due to spurious phase calibration signals (see, Rogers, 1991). As we have stated, a large
 676 fraction of the systematic differences between group delay and phase delay observables
 677 attributes to group delay observables. It is important to identify the causes of these
 678 systematic differences, as group delays are the basic observables of geodetic VLBI.
 679 However, any conclusion on this effect needs further investigations.

680 (7) *Polarization-related effects* The polarization leakage (Martí-Vidal et al., 2021)
 681 can have different impacts between the observations of the legacy S/X and the mixed
 682 modes. The visibility of $RH+RV$ from the mixed mode session is not able to minimize
 683 the impact of the D term as is the pseudo-Stoke I visibility constructed for the dual
 684 linear polarizations in VGOS; without being calibrated, there may be significant errors.
 685 However, the short baselines with more than two sessions available were observed in
 686 the legacy S/X mode. The results so far do not allow us to assess the potential errors
 687 in the mixed mode of the circularly polarized receivers and the linearly polarized
 688 receivers. The only information that we presently have is that the residual level of the
 689 mixed mode observables of baselines ONSALA60–ONSA13NE and ONSALA60–ONSA13SW is
 690 about 5.0 ps and that of baseline ONSA13NE–ONSA13SW, both of which observed with
 691 the linearly polarized receivers, is only 2.0 ps based on the data analyses of the two
 692 mixed mode sessions. However, the former two baselines are about five times longer,
 693 which prevents us from making any conclusion so far. We leave these effects for a later
 694 investigation.

695 (8) *Source positions* The short baselines in this study are sensitive to source struc-
 696 ture only at the sub-arcsecond level or larger, three orders of magnitude greater than
 697 the typical uncertainties of source positions in the third realization of the International
 698 Celestial Reference Frame (ICRF3; Charlot et al., 2020). In general, source positions
 699 are not estimated in data analysis of short-baseline observations, as one would keep
 700 the number of model parameters to a minimum to obtain robust solutions. Due to
 701 radio interferometry, source structure at the arc-second scales is resolved out and not
 702 detected by the long baselines of thousands of kilometers. The source positions in the
 703 ICRF3, determined primarily from long-baseline observations, were used as a priori
 704 and not estimated in our solutions. However, the ICRF3 source positions can be differ-
 705 ent from the reference positions for the short baselines due to large scale structure for
 706 some of the sources. Even though we have stated that these effects should be small for
 707 most of the geodetic sources, the magnitude should be properly quantified by actual
 708 observations.

709 We analyzed the VLBI sessions of station position tie carried out at the Onsala
 710 site, the ONTIE sessions (Varenius et al., 2021). The advantages of these ONTIE
 711 sessions for this particular investigation are the large number of scans (~ 1200 scans
 712 per session) and the multiple short baselines formed by the three antennas at the
 713 site; they allow us to obtain robust solutions for estimating a large number of source
 714 position parameters. For instance, session 20NOV12VB observed 126 sources with
 715 3522 observations in total. With the parameterization of one-hour-interval PWL func-
 716 tions for both the dZWDs and the clocks of antennas ONSA13NE and ONSA13SW and
 717 the positions of the two antennas, the WRMS delay residual is 2.9 ps based on 3442
 718 used phase delays. The formal errors of station position estimates are 0.2 mm in the
 719 up direction and 0.05 mm in the horizontal directions. In another solution, we esti-

720 mated right ascension and declination for the 105 sources with more than ten phase
 721 delays together with the same parameters in the previous solution. The WRMS delay
 722 residual is 2.7 ps from the solution of estimating source positions; however, the formal
 723 errors of station position estimates increase by 50% in the up direction and by 100%
 724 in the horizontal directions. The differences in station position estimates are about
 725 0.1 mm in the up direction and 0.2 mm in the two horizontal directions, a demonstra-
 726 tion that errors in source positions affect the horizontal directions rather than the up
 727 direction for the ties. The results from other ONTIE sessions are similar to that of
 728 session 20NOV12VB presented here. Radio sources observed in the ONTIE sessions
 729 are from the same source catalog of the IVS observations; thus, it is reasonable to
 730 conclude that the impact of source position differences due to large scale structure
 731 may be about 0.2 mm on the horizontal directions. This is insignificant relative to
 732 the uncertainties and probably will not cause systematic changes in position estimates
 733 but only increase the scatters. There is no intention either to observe the same set
 734 of sources or to observe a given source at the same Greenwich mean sidereal time in
 735 different sessions, therefore, this error source is non-repeatable (i.e., a random error as
 736 opposed to a systematic error).

737 (9) *Atmospheric effects* In order to separate the elevation-dependent effects of
 738 the atmosphere from the estimates of station positions, in particular the Up compo-
 739 nent, geodetic VLBI observations rapidly switch between radio sources at different
 740 directions. Fortunately, atmospheric effects are greatly canceled for short baselines
 741 and the hydrostatic part of the effects is modeled in our solutions. The residual effects
 742 are investigated and discussed here.

743 Based on phase delays of WETT13N–WETTZELL in the 107 sessions, we performed
 744 three sets of solutions: (1) estimating dZWDs with a time interval of PWL of 1 hour,
 745 (2) estimating dZWDs with a time interval of 24 hours, and (3) not estimating dZWDs.
 746 Differences in the mean estimates of the horizontal components are negligible, smaller
 747 than 0.01 mm, between these three sets of solutions, and the mean of the differences
 748 in the Up component is 0.05 ± 0.05 mm between estimating dZWDs with two different
 749 time intervals. However, the mean of the differences in the Up estimates between esti-
 750 mating dZWDs (with a time interval of either 24 hours or 1 hour) and not estimating is
 751 -1.1 ± 0.1 mm. The residual time series of the Up estimates from the three sets of solu-
 752 tions are shown in Fig. 8. Seasonal variations with a magnitude larger than 1 mm occur
 753 in the Up residuals when the dZWDs were estimated. Even though the atmospheric
 754 turbulence due to wet troposphere on the local scale is believed to have detectable
 755 effects in VLBI observables (see, e.g., [Treuhaft & Lanyi, 1987](#)), our results suggest
 756 that the baseline time series can be stabilized by not estimating the atmospheric ef-
 757 fects in the case of the short baseline WETT13N–WETTZELL. Through the investigation,
 758 we conclude that the impact of atmospheric effects on the baseline ties from short-
 759 baseline observations is negligible in the horizontal components but can be 1–2 mm in
 760 the Up component. This amount of impact may be inevitable and prevalence in the
 761 current VLBI products because the signal propagation delays due to water vapour are
 762 always estimated in geodetic solutions of VLBI observations. The study may suggest
 763 that achieving global geodetic accuracy of 1 mm with VGOS will have to rely on
 764 corrections for the water vapour-induced delays from independent instruments, such
 765 as collocated microwave radiometers (see, e.g., [Forkman et al., 2021](#)).

766 6 Potential applications of phase delays from long baselines

767 We have demonstrated that phase delays can be used (1) to investigate the
 768 systematic errors of group delays and (2) to derive geodetic results of baseline vectors.
 769 However, the study has limited to utilizing these observables from short baselines,
 770 mainly due to the challenge in resolving phase ambiguities for long baselines. In this

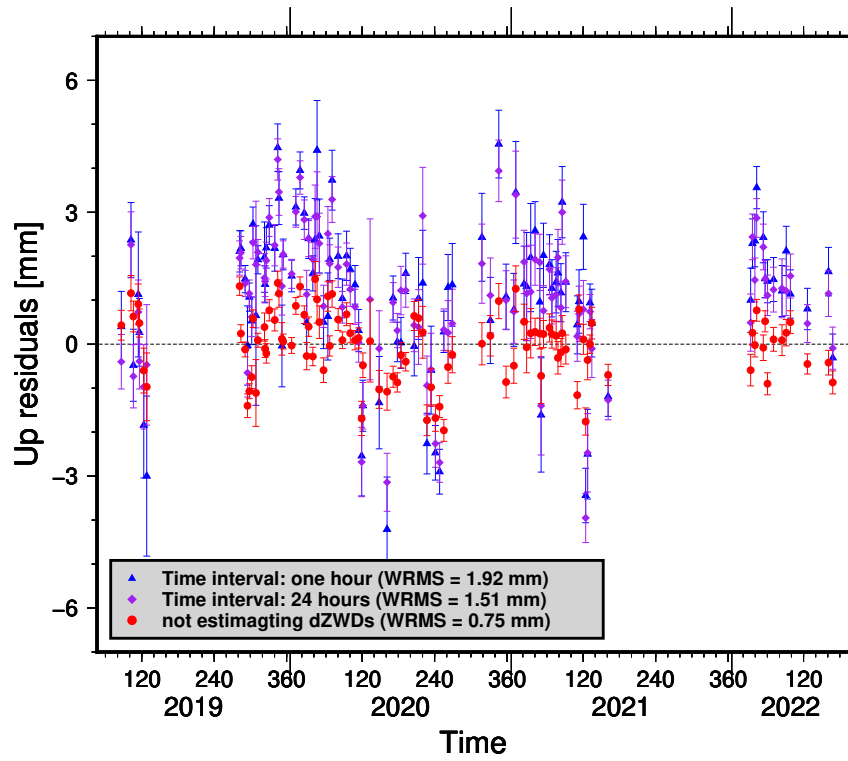


Figure 8. Comparison of the Up residuals from solutions with three different treatments of the atmospheric effects: estimating with a time interval of 1 hour for PWL (blue triangles), estimating with a time interval of 24 hours (purple rhombuses), and not estimating (red dots). The black dash line indicate the mean Up position obtained from the solutions without estimating ZWDs, which is the reference for calculating the Up residuals of all the three types of solutions.

771 section, we will briefly discuss the potential application of phase delays from long
772 baselines.

773 As discussed in section 2.2 in detail, the methods of resolving phase ambiguities
774 include: (1) directly employing group delays to predict the phase ambiguities, (2)
775 using theoretical model delays, and (3) relying on geodetic solutions of group delays.
776 Because typically instrumental effects can introduce large systematic errors in the iono-
777 spheric corrections determined from S/X-band group delays (e.g., constant offsets) and
778 resolving phase ambiguities for long baselines requires a special attention to the differ-
779 ence in the reference frequencies of these corrections between group delays and phase
780 delays (e.g., the constant offsets can introduce large variations due to the changes in
781 the reference frequencies of the corrections from group delays), neither of these three
782 options could work well for long baselines in the legacy VLBI observations. In the
783 VGOS observations, however, because the ionospheric effects are simultaneously esti-
784 mated with group delays and visibility phases in the broadband fringe fitting process
785 (Cappallo, 2014), this naturally resolves the challenge of predicting phase ambiguities
786 caused by the ionospheric effects. The VGOS phase delays are recently discussed and
787 investigated by the IVS VGOS Technical Committee, and their potential applications
788 can be to improve the quality of the group delays and to investigate the effects of
789 source structure (Xu et al., 2022) with the goal of improving the geodetic products
790 from VGOS. We remark that without mitigating the systematic errors caused by, e.g.,
791 water vapour and source structure, the higher precision of phase delays alone cannot
792 promise significantly better geodetic products in general cases of long baselines.

793 7 Summary

794 We have analyzed the phase delays in the IVS routine global observations for the
795 short baselines at eight geodetic VLBI sites to derive the station position ties with high
796 accuracy. The results of the baseline vector WETTZ13N–WETTZELL have baseline repeata-
797 bilities of better than 1 mm in all the three directions. The potential systematic errors
798 were investigated and discussed in the study. As demonstrated by the investigation
799 of the cable delay corrections, instrumental effects typically can introduce errors with
800 a magnitude larger than 1 mm in station position estimates. The atmospheric effects,
801 which are always estimated in geodetic solutions, may also cause seasonal fluctuations
802 at the a few mm level in station position time series.

803 Phase delays produce significantly better determinations of the baseline vectors
804 than the linearly combined group delays at S/X bands. An independent solution of
805 only short-baseline observables does not suffer from some of the errors in long-baseline
806 observables. The phase delay results of the position ties can be directly used in the
807 data analysis of legacy S/X observations and VGOS observations or the combined
808 analysis of both observations. Nevertheless, it should be noted that there currently
809 exists incompatibility in applying these phase delay results to the routine data analysis
810 based on group delays since some antenna pairs have significantly different position
811 ties between group delays and phase delays. When the VLBI phase delay results are
812 used for studies with other space techniques (see, e.g., Ning et al., 2015; Glaser et
813 al., 2019), an attention should be paid to take the systematic, repeatable errors into
814 account, in particular the up coordinate.

815 Acknowledgments

816 The results reported in this paper used the data coordinated by the International VLBI
817 Service (IVS) and its international self-funded member organizations. We are grateful
818 to the IVS stations at Hartebeesthoek (South Africa Radio Astronomical Observa-
819 tory), Ishioka (Geospatial Information Authority of Japan), Kokee Park (U.S. Naval
820 Observatory and NASA GSFC, USA), Ny-Ålesund (Norwegian Mapping Authority,

821 Norway), Onsala (Onsala Space Observatory, Chalmers University of Technology, Swe-
 822 den), Shanghai (Shanghai Astronomical Observatory, China), Wettzell (Bundesamt
 823 für Kartographie und Geodäsie and Technische Universität München, Germany), and
 824 Yebes (Instituto Geográfico Nacional, Spain), to the staff at the Bonn Correlator, the
 825 Washington Correlator, the Onsala Observatory Correlator, and the MIT Haystack
 826 Observatory correlator for performing the correlations and the fringe fitting of the
 827 data, to the NASA GSFC VLBI group and the BKG VLBI group for doing the geode-
 828 tic solutions, and to the IVS Data Centers at BKG (Leipzig, Germany), Observatoire
 829 de Paris (France), and NASA CDDIS (Greenbelt, MD, USA) for the central data
 830 holds.

831 This research has made use of the Generic Mapping Tools package, the pgplot
 832 library, and the SAO/NASA Astrophysics Data System. The work was supported by
 833 the Academy of Finland project No. 315721.

834 References

- 835 Altamimi, Z., Rebischung, P., Métivier, L., & Collilieux, X. (2016). ITRF2014:
 836 A new release of the International Terrestrial Reference Frame modeling non-
 837 linear station motions. *Journal of Geophysical Research (Solid Earth)*, *121*(8),
 838 6109-6131. doi: 10.1002/2016JB013098
- 839 Anderson, J. M., & Xu, M. H. (2018). Source Structure and Measurement Noise Are
 840 as Important as All Other Residual Sources in Geodetic VLBI Combined. *Jour-
 841 nal of Geophysical Research (Solid Earth)*, *123*(11), 10,162-10,190. doi: 10.1029/
 842 2018JB015550
- 843 Baver, K., & Gipson, J. (2020). Balancing source strength and sky coverage in IVS-
 844 INT01 scheduling. *Journal of Geodesy*, *94*(2), 18. doi: 10.1007/s00190-020-01343
 845 -1
- 846 Bergstrand, S., Herbertsson, M., Rieck, C., Spetz, J., Svantesson, C.-G., & Haas, R.
 847 (2019). A gravitational telescope deformation model for geodetic VLBI. *Journal
 848 of Geodesy*, *93*(5), 669-680. doi: 10.1007/s00190-018-1188-1
- 849 Cappallo, R. (2014, Dec). Correlating and Fringe-fitting Broadband VGOS
 850 Data. In *International vlbi service for geodesy and astrometry 2014 general
 851 meeting proceedings: "vgos: The new vlbi network* (p. 91-96). Retrieved from
 852 <https://ivsc.gsfc.nasa.gov/publications/gm2014/019-Cappallo.pdf>
- 853 Carter, W. E., Rogers, A. E. E., Counselman, C. C., & Shapiro, I. I. (1980).
 854 Comparison of geodetic and radio interferometric measurements of the
 855 Haystack-Westford base line vector. *JGR*, *85*(B5), 2685-2687. doi: 10.1029/
 856 JB085iB05p02685
- 857 Charlot, P., Jacobs, C. S., Gordon, D., Lambert, S., de Witt, A., Böhm, J., Fey,
 858 A. L., Heinkelmann, R., Skurikhina, E., Titov, O., Arias, E. F., Bolotin, S.,
 859 Bourda, G., Ma, C., Malkin, Z., Nothnagel, A., Mayer, D., MacMillan, D. S.,
 860 Nilsson, T., & Gaume, R. (2020). The third realization of the International
 861 Celestial Reference Frame by very long baseline interferometry. *Astronomy and
 862 Astrophysics*, *644*, A159. doi: 10.1051/0004-6361/202038368
- 863 Forkman, P., Flygare, J., & Elgered, G. (2021). Water vapour radiometry in geode-
 864 tic very long baseline interferometry telescopes: assessed through simulations.
 865 *Journal of Geodesy*, *95*(11), 117. doi: 10.1007/s00190-021-01571-z
- 866 Diamantidis, P.-K., Kłopotek, G., & Haas, R. (2021). VLBI and GPS inter- and
 867 intra-technique combinations on the observation level for evaluation of TRF and
 868 EOP. *Earth, Planets, and Space*, *73*(1), 68. doi: 10.1186/s40623-021-01389-1
- 869 Glaser, S., König, R., Neumayer, K. H., Nilsson, T., Heinkelmann, R., Flechtner,
 870 F., & Schuh, H. (2019). On the impact of local ties on the datum realization
 871 of global terrestrial reference frames. *Journal of Geodesy*, *93*(5), 655-667. doi:
 872 10.1007/s00190-018-1189-0

- 873 Halsig, S., Bertarini, A., Haas, R., Iddink, A., Kodet, J., Kronschnabl, G., Neid-
874 hardt, A., Nothnagel, A., Plötz, C., & Schüler, T. (2019). Atmospheric refraction
875 and system stability investigations in short-baseline VLBI observations. *Journal of*
876 *Geodesy*, 93(4), 593-614. doi: 10.1007/s00190-018-1184-5
- 877 Herring, T. A. (1992). Submillimeter horizontal position determination using very
878 long baseline interferometry. *JGR*, 97(B2), 1981-1990. doi: 10.1029/91JB02649
- 879 Hill, E. M., Davis, J. L., Elósegui, P., Wernicke, B. P., Malikowski, E., & Niemi,
880 N. A. (2009). Characterization of site-specific GPS errors using a short-
881 baseline network of braced monuments at Yucca Mountain, southern Nevada.
882 *Journal of Geophysical Research (Solid Earth)*, 114(B11), B11402. doi:
883 10.1029/2008JB006027
- 884 King, M. A., & Williams, S. D. P. (2009). Apparent stability of GPS monumen-
885 tation from short-baseline time series. *Journal of Geophysical Research (Solid*
886 *Earth)*, 114(B10), B10403. doi: 10.1029/2009JB006319
- 887 Lösler, M., Haas, R., Eschelbach, C., & Greiwe, A. (2019). Gravitational de-
888 formation of ring-focus antennas for VGOS: first investigations at the On-
889 sala twin telescopes project. *Journal of Geodesy*, 93(10), 2069-2087. doi:
890 10.1007/s00190-019-01302-5
- 891 Martí-Vidal, I., Mus, A., Janssen, M., de Vicente, P., & González, J. (2021). Polar-
892 ization calibration techniques for the new-generation VLBI. *Astronomy and Astro-*
893 *physics*, 646, A52. doi: 10.1051/0004-6361/202039527
- 894 Niell, A., Whitney, A., Petrachenko, W., Schlüter, W., Vandenberg, N., Hase,
895 H., Koyama, Y., Ma, C., Schuh, H., & Tuccari, G. (2007). VLBI2010: a
896 Vision for Future Geodetic VLBI. In P. Tregoning & C. Rizos (Eds.), *Dy-*
897 *namic planet - monitoring and understanding a dynamic planet with geode-*
898 *tic and oceanographic tools, edited by paul tregoning and chris rizos. isbn isbn*
899 *978-3-540-49349-5. berlin: Springer, 2007., p.757 (p. 757). Retrieved from*
900 https://link.springer.com/chapter/10.1007/978-3-540-49350-1_108
- 901 Niell, A. E., Barrett, J. P., Cappallo, R. J., Corey, B. E., Elosegui, P., Mondal, D.,
902 Rajagopalan, G., Rusczyk, C. A., & Titus, M. A. (2021). VLBI measurement of
903 the vector baseline between geodetic antennas at Kokee Park Geophysical Obser-
904 vatory, Hawaii. *Journal of Geodesy*, 95(6), 65. doi: 10.1007/s00190-021-01505-9
- 905 Ning, T., Haas, R., & Elgered, G. (2015). Determination of the local tie vector be-
906 tween the VLBI and GNSS reference points at Onsala using GPS measurements.
907 *Journal of Geodesy*, 89(7), 711-723. doi: 10.1007/s00190-015-0809-1
- 908 Nothnagel, A. (2009). Conventions on thermal expansion modelling of radio tele-
909 scopes for geodetic and astrometric VLBI. *Journal of Geodesy*, 83(8), 787-792.
910 doi: 10.1007/s00190-008-0284-z
- 911 Nothnagel, A., Artz, T., Behrend, D., & Malkin, Z. (2017). International VLBI Ser-
912 vice for Geodesy and Astrometry. Delivering high-quality products and embarking
913 on observations of the next generation. *Journal of Geodesy*, 91(7), 711-721. doi:
914 10.1007/s00190-016-0950-5
- 915 Nothnagel, A., Holst, C., & Haas, R. (2019). A VLBI delay model for grav-
916 itational deformations of the Onsala 20 m radio telescope and the impact
917 on its global coordinates. *Journal of Geodesy*, 93(10), 2019-2036. doi:
918 10.1007/s00190-019-01299-x
- 919 Petrachenko, B., Niell, A., Behrend, D., Corey, B., Boehm, J., Charlot, P., Collioud,
920 A., Gipson, J., Haas, R., Hobiger, T., Koyama, Y., MacMillan, D., Malkin, Z.,
921 Nilsson, T., Pany, A., Tuccari, G., Whitney, A., & Wresnik, J. (2009). *Design As-*
922 *pects of the VLBI2010 System. Progress Report of the IVS VLBI2010 Committee,*
923 *June 2009. NASA/TM-2009-214180.*
- 924 Phogat, A., Kronschnabl, G., Pltz, C., Schwarz, W., & Schler, T. (2018). Short base-
925 line observations at geodetic observatory wettzell. *Data*, 3(4). Retrieved from
926 <https://www.mdpi.com/2306-5729/3/4/64> doi: 10.3390/data3040064

- 927 Ray, J. R., & Corey, B. E. (1991). Current Precision of VLBI Multi-Band Delay
928 Observables. In *Geodetic vlbi: Monitoring global change* (p. 123). Retrieved
929 from [https://www.ngs.noaa.gov/PUBS_LIB/Proceedings_of_AGU_Chapman](https://www.ngs.noaa.gov/PUBS_LIB/Proceedings_of_AGU_Chapman_Conference_on_Geodetic_VLBI_TM_NOS137_NGS49.pdf)
930 [_Conference_on_Geodetic_VLBI_TM_NOS137_NGS49.pdf](https://www.ngs.noaa.gov/PUBS_LIB/Proceedings_of_AGU_Chapman_Conference_on_Geodetic_VLBI_TM_NOS137_NGS49.pdf)
- 931 Robertson, D. S., Carter, W. E., Campbell, J., & Schuh, H. (1985). Daily Earth
932 rotation determinations from IRIS very long baseline interferometry. *Nature*,
933 *316*(6027), 424-427. doi: 10.1038/316424a0
- 934 Rogers, A. E. E. (1991). Instrumentation Improvements to Achieve Millimeter
935 Accuracy (Keynote Presentation). In *Geodetic vlbi: Monitoring global change*
936 (p. 1). Retrieved from [https://www.ngs.noaa.gov/PUBS_LIB/Proceedings_of](https://www.ngs.noaa.gov/PUBS_LIB/Proceedings_of_AGU_Chapman_Conference_on_Geodetic_VLBI_TM_NOS137_NGS49.pdf)
937 [_AGU_Chapman_Conference_on_Geodetic_VLBI_TM_NOS137_NGS49.pdf](https://www.ngs.noaa.gov/PUBS_LIB/Proceedings_of_AGU_Chapman_Conference_on_Geodetic_VLBI_TM_NOS137_NGS49.pdf)
- 938 Rothacher, M., Angermann, D., Artz, T., Bosch, W., Drewes, H., Gerstl, M., Kelm,
939 R., König D., König R., Meisel H., Müller H., Nothnagel A., Panafidina N.,
940 Richter B., Rudenko S., Schwegmann W., Seitz M., Steigenberger P., Tesmer
941 S., Tesmer V., & Thaller, D. (2011). GGOS-D: homogeneous reprocessing and
942 rigorous combination of space geodetic observations. *Journal of Geodesy*, *85*(10),
943 679-705. doi: 10.1007/s00190-011-0475-x
- 944 Schartner, M., Kern, L., Nothnagel, A., Böhm, J., & Soja, B. (2021). Optimal
945 VLBI baseline geometry for UT1-UTC Intensive observations. *Journal of Geodesy*,
946 *95*(7), 75. doi: 10.1007/s00190-021-01530-8
- 947 Schuh, H., & Behrend, D. (2012). VLBI: A fascinating technique for geodesy and as-
948 trometry. *Journal of Geodynamics*, *61*, 68-80. doi: 10.1016/j.jog.2012.07.007
- 949 Schüller, T., Kronschnabl, G., Plötz, C., Neidhardt, A., Bertarini, A., Bernhart, S.,
950 la Porta, L., Halsig, S., & Nothnagel, A. (2015). Initial Results Obtained with
951 the First TWIN VLBI Radio Telescope at the Geodetic Observatory Wettzell.
952 *Sensors*, *15*(8), 18767-18800. doi: 10.3390/s150818767
- 953 Sekido, M., Takefuji, K., Ujihara, H., Kondo, T., Tsutsumi, M., Kawai, E., Hachisu,
954 H., Nemitz, N., Pizzocaro, M., Clivati, C., Perini, F., Negusini, M., Maccaferri,
955 G., Ricci, R., Roma, M., Bortolotti, C., Namba, K., Komuro, J., Ichikawa, R.,
956 Suzuyama, T., Watabe, K., Leute, J., Petit, G., Calonico, D., & Ido, T. (2021). A
957 broadband VLBI system using transportable stations for geodesy and metrology:
958 an alternative approach to the VGOS concept. *Journal of Geodesy*, *95*(4), 41. doi:
959 10.1007/s00190-021-01479-8
- 960 Sovers, O. J., Fanselow, J. L., & Jacobs, C. S. (1998). Astrometry and geodesy with
961 radio interferometry: experiments, models, results. *Reviews of Modern Physics*,
962 *70*(4), 1393-1454. doi: 10.1103/RevModPhys.70.1393
- 963 Treuhaft, R. N., & Lanyi, G. E. (1987). The effect of the dynamic wet troposphere
964 on radio interferometric measurements. *Radio Science*, *22*(02), 251-265. doi: 10
965 .1029/RS022i002p00251
- 966 Teke, K., Nilsson, T., Böhm, J., Hobiger, T., Steigenberger, P., García-Espada,
967 S., ... Willis, P. (2013). Troposphere delays from space geodetic techniques,
968 water vapor radiometers, and numerical weather models over a series of con-
969 tinuous VLBI campaigns. *Journal of Geodesy*, *87*(10-12), 981-1001. doi:
970 10.1007/s00190-013-0662-z
- 971 Thompson, A. R., Moran, J. M., & Swenson, J., George W. (2017). *Interferometry*
972 *and Synthesis in Radio Astronomy, 3rd Edition*. doi: 10.1007/978-3-319-44431-4
- 973 Varenius, E., Haas, R., & Nilsson, T. (2021). Short-baseline interferometry local-tie
974 experiments at the Onsala Space Observatory. *Journal of Geodesy*, *95*(5), 54. doi:
975 10.1007/s00190-021-01509-5
- 976 Xu, M. H., Anderson, J. M., Heinkelmann, R., Lunz, S., Schuh, H., & Wang, G.
977 (2021). Observable quality assessment of broadband very long baseline interferom-
978 etry system. *Journal of Geodesy*, *95*(5), 51. doi: 10.1007/s00190-021-01496-7
- 979 Xu, M. H., Anderson, J. M., Heinkelmann, R., Lunz, S., Schuh, H., & Wang,
980 G. L. (2019). Structure Effects for 3417 Celestial Reference Frame Ra-

- 981 dio Sources. *The Astrophysical Journal Supplement Series*, 242(1), 5. doi:
 982 10.3847/1538-4365/ab16ea
- 983 Xu, M. H., Heinkelmann, R., Anderson, J. M., Mora-Diaz, J., Schuh, H., &
 984 Wang, G. L. (2016). The Source Structure of 0642+449 Detected from
 985 the CONT14 Observations. *The Astronomical Journal*, 152(5), 151. doi:
 986 10.3847/0004-6256/152/5/151
- 987 Xu, M. H., Savolainen, T., Anderson, J. M., Kareinen, N., Zubko, N., Lunz, S.,
 988 & Schuh, H. (2022). Impacts of the image alignment over frequency for
 989 VLBI Global Observing System. *Astronomy and Astrophysics (in press)*. doi:
 990 <https://doi.org/10.1051/0004-6361/202140840>
- 991 Xu, M. H., Savolainen, T., Zubko, N., Poutanen, M., Lunz, S., Schuh, H., & Wang,
 992 G. L. (2021). Imaging VGOS Observations and Investigating Source Structure
 993 Effects. *Journal of Geophysical Research (Solid Earth)*, 126(4), e21238. doi:
 994 10.1029/2020JB021238